Journal of Human Evolution 172 (2022) 103253

Contents lists available at ScienceDirect

Journal of Human Evolution

journal homepage: www.elsevier.com/locate/jhevol

Comparing the Boxgrove and Atapuerca (Sima de los Huesos) human fossils: Do they represent distinct paleodemes?

Annabelle L. Lockey [a, b], Laura Rodríguez [c, d], Laura Martín-Francés [e, f, g, h], Juan Luis Arsuaga [e, f, i], José María Bermúdez de Castro [a, g], Lucile Crété [j, *], María Martinón-Torres [a, g], Simon Parfitt [j, k], Matt Pope [k], Chris Stringer [j]

[a] Department of Anthropology, University College London, 14 Taviton Street, London, WC1H 0BW, UK
[b] Paleoanthropology, Senckenberg Center for Human Evolution and Paleoenvironment, Universität Tübingen, 72070, Germany
[c] Área de Antropología Física, Departamento de Biodiversidad y Gestión Ambiental, Facultad de Ciencias Biologicas y Ambientales, Universidad de León. Campus de Vegazana s/n, 24071 León, Spain
[d] Laboratorio de Evolución Humana, Departamento de Historia, Geografía y Comunicación, Facultad de Humanidades y Comunicación, Universidad de Burgos, Edificio I+D+i, Plaza Misael Bañuelos s/n, C/ Villadiego s/n, 09001, Burgos, Spain
[e] Departamento de Geodinámica, Estratigrafía y Paleontología, Facultad de Ciencias Geológicas, Universidad Complutense de Madrid, 28040, Madrid, Spain
[f] Centro Mixto (UCM-ISCIII) de Evolución y Comportamiento Humanos, Av. Monforte de Lemos 5, 28029, Madrid, Spain
[g] National Research Center on Human Evolution (CENIEH), Paseo Sierra de Atapuerca 3, 09002, Burgos, Spain
[h] Institut Català de Paleoecologia Humana i Evolució Social (IPHES-CERCA), Zona Educacional 4, Campus Sescelades URV (Edifici W3), 43007, Tarragona, Spain
[i] Cátedra de Bioacústica Evolutiva y Paleoantropología (HM Hospitales – Universidad de Alcalá), Área de Antropología Física, Departamento de Ciencias de la Vida, Universidad de Alcalá, 28871, Alcalá de Henares, Madrid, Spain
[j] Centre for Human Evolution Research (CHER), The Natural History Museum, London, SW7 5BD, UK
[k] Institute of Archaeology, University College London, 31-34 Gordon Square, London, WC1H 0PY, UK

ARTICLE INFO

Article history:
Received 1 April 2021
Accepted 17 August 2022
Available online xxx

Keywords:
Human evolution
Europe
Pleistocene
Hominin
Incisor
Tibia

ABSTRACT

The early Middle Pleistocene human material from Boxgrove (West Sussex, UK) consists of a partial left tibia and two lower incisors from a separate adult individual. These remains derive from deposits assigned to the MIS 13 interglacial at about 480 ka and have been referred to as *Homo* cf. *heidelbergensis*. The much larger skeletal sample from the Sima de los Huesos (Atapuerca, Spain) is dated to the succeeding MIS 12, at about 430 ka. This fossil material has previously been assigned to *Homo heidelbergensis* but is now placed within the Neanderthal clade. Because of the scarcity of human remains from the Middle Pleistocene and their morphological variability, this study assessed whether the Boxgrove specimens fit within the morphological variability of the homogeneous Sima de los Huesos population. Based on morphometric analyses performed against 22 lower incisors from Sima de los Huesos and published material, the data from the Boxgrove incisors place them comfortably within the range of Sima de los Huesos. Both assemblages present robust incisors distinct from the overall small recent *Homo sapiens* incisors, and Boxgrove also aligns closely with *Homo neanderthalensis* and some other European Middle Pleistocene hominins. Following morphological and cross-sectional analyses of the Boxgrove tibia compared to seven adult Sima de los Huesos specimens and a set of comparative tibiae, Boxgrove is shown to be similar to Sima de los Huesos and Neanderthals in having thick cortices and bone walls, but in contrast resembles modern humans in having a straight anterior tibial crest and a suggestion of a lateral concavity. Based on the patterns observed, there is no justification for assigning the Boxgrove and Sima de los Huesos incisors to distinct paleodemes, but the tibial data show greater contrasts and suggest that all three of these samples are unlikely to represent the same paleodeme.

* Corresponding author.
E-mail address: l.crete@nhm.ac.uk (L. Crété).

https://doi.org/10.1016/j.jhevol.2022.103253

1. Introduction

Despite the scarcity and fragmentary nature of the Middle Pleistocene (MP) hominin fossil record, recent studies have increased our knowledge of human evolution in Europe, revealing a complex picture of settlement patterns and population diversity. In particular, the morphological and metric variability observed among MP hominins, as well as the improved geochronological data available for key MP fossil localities (e.g., Nomade et al., 2011; Rink et al., 2013; Falguères et al., 2015; Daura et al., 2017; Demuro et al., 2019; Harvati et al., 2019), have led to much debate on the taxonomy of certain specimens, as well as on the origin of the Neanderthal lineage. Although a European origin and local evolution for the Neanderthals is supported by many researchers (Dean et al., 1998; Hublin, 2009; Stringer, 2011; Arsuaga et al., 2014), debate remains about the anagenetic (linear) or cladogenetic (splitting) evolutionary origin of this clade (Stringer, 2012; Arsuaga et al., 2014; Daura et al., 2017). Indeed, while some have argued that Neanderthals might have evolved out of *Homo heidelbergensis* in Europe (Rightmire, 2008; Stringer, 2012), others have suggested that there were several populations (paleodemes) of hominins present in Europe throughout the MP, some of them evolving toward the classic Neanderthal morphology and others not (Demuro et al., 2019). This latter hypothesis is based on the mosaic of primitive and derived features displayed in various MP samples, where Neanderthal autapomorphies do not seem to appear in the fossil record following a gradual and linear model (Bermúdez de Castro et al., 2016, 2018; Zanolli et al., 2018; Demuro et al., 2019). For instance, the near-contemporaneous southwestern European sites of Aroeira, Atapuerca-Sima de los Huesos (SH), and Arago yielded hominin fossils of differing morphologies, suggesting that high diversity within or between MP paleodemes likely characterized the region at the time, potentially due to complex population dynamics with varying levels of isolation and admixture (Dennell et al., 2011; Arsuaga et al., 2014; Daura et al., 2017). Recent mitochondrial paleogenetic data also showed a complex pattern of population relationships through space and time during the MP, in particular between the Sima de los Huesos hominins, the Neanderthals, and the Denisovans (Meyer et al., 2014, 2016; Kuhlwilm et al., 2016). However, genomic data confirmed the SH population relationship with the Neanderthals.

Within the scarce and fragmentary MP hominin fossil record, the partial tibia and the two lower incisors from Boxgrove (West Sussex, UK) provide valuable data for the assessment of hominin morphological diversity, as these remains derive from deposits attributed to the cooling limb of the MIS 13 interglacial, at about 480 ka (Preece and Parfitt, 2012; Whittaker and Parfitt, 2017). These fossils are younger than the key MP hominin mandible from Mauer, holotype of *H. heidelbergensis* (Schoetensack, 1908), dated to about 609 ka (likely MIS 15; Wagner et al., 2010), and closer in age to the SH and Arago fossils, dated to MIS 12 (Falguères et al., 2015; Demuro et al., 2019). Previous morphological (Stringer et al., 1998) and biomechanical (Trinkaus et al., 1999) studies of the Boxgrove 1 tibia highlighted similarities to other Pleistocene archaic *Homo* tibiae, particularly in its external morphology and overall robusticity (Trinkaus, 2009), with diaphyseal strength and/or cold-adapted body proportions paralleling those of the Neanderthals. Morphological and metrical analyses of the Boxgrove 2 and 3 incisors (Hillson et al., 2010) showed that these compared well with other European MP mandibular incisors, such as those in the Mauer mandible, with a robust crown and root (see Hillson et al., 2010 for further description). Based on the various characters observed on the Boxgrove hominin material, the remains have been referred to *Homo* cf. *heidelbergensis* (Roberts et al., 1994; Stringer et al., 1998; Hillson et al., 2010), although the taxonomic status of *H. heidelbergensis* remains debated (Stringer, 1983, 2012; Mounier et al., 2009; Mounier and Caparros, 2015; Roksandic et al., 2018). In this article, we compare the dental and tibial morphology of the Boxgrove specimens to samples from the broadly contemporary assemblage from SH to assess morphological diversity in the European MP hominin fossil record and discuss the validity of assigning the Boxgrove and SH material to distinct paleodemes.

As the largest hominin collection currently available for the MP, the SH material has been extensively studied, allowing the analysis of intrapopulation variability (Arsuaga et al., 1997; Lorenzo et al., 1998; Bermúdez de Castro et al., 2004; Gómez-Olivencia et al., 2007; Prado-Simón et al., 2012), and demonstrating that Neanderthal autapomorphies were present in all skeletal elements of this population (Arsuaga et al., 2015; Quam et al., 2016; Rodríguez et al., 2016; Martín-Albaladejo et al., 2017; Pablos et al., 2017). As such, while these remains were previously assigned to *H. heidelbergensis* (Arsuaga et al., 1997), they have since been placed within the Neanderthal clade based on both morphology and ancient DNA (Arsuaga et al., 2014; Meyer et al., 2016), and are the earliest known paleodeme exhibiting clear Neanderthal features (Demuro et al., 2019). The highly derived state of the SH population observed through such studies raised questions regarding the degree of intra- and interpopulation variability existing during the MP, and highlighted the need for further studies to assess whether the SH assemblage could be seen as representative of European MP populations, or whether it should be considered as a distinct paleodeme.

Although the morphology of lower incisors of extinct and extant *Homo* has been reported to be less discriminative for taxonomic purposes than that of posterior teeth (Skinner et al., 2015; Martín-Francés et al., 2018; Zanolli et al., 2018; Lockey et al., 2020), methodological advances have permitted the study of dental tissue proportions and provide additional avenues to assist taxonomic assessment (e.g., Smith et al., 2003, 2012; Olejniczak et al., 2008; Macchiarelli et al., 2013; Zanolli and Mazurier, 2013; Pan et al., 2016; Martín-Francés et al., 2018, 2020). For instance, previous work has shown that the anterior dental tissue proportions and dimensions for Neanderthals are distinct from other extinct hominins and extant recent modern humans (RMH; Smith et al., 2012; Le Cabec et al., 2013; Buti et al., 2017), with the SH canines exhibiting a dental tissue proportion pattern typical of Neanderthals (García-Campos et al., 2019). Evaluating and comparing the endostructure of the mandibular incisors from the Boxgrove and SH specimens can thus provide additional data to assess whether these hominins align with Neanderthals, RMH, or present unique patterns of dental tissue proportions or root dimensions.

Previous work has described the morphology of the Boxgrove tibia (Stringer et al., 1998), highlighting its rounded and straight anterior crest, with only a suggestion of a lateral concavity, thus distinguishing it from that of Neanderthals. This study also provided an estimate of the articular length of Boxgrove 1 at 370 and 376 mm (mean = 373 mm). Because living bone responds to mechanical loading, especially during development, detailed analyses of long bone morphology and inner structure can thus indirectly inform us about the activity, sex, and size of individuals (Ruff and Hayes, 1983; Ruff et al., 1993, 1994). Cross-sectional shape and thickness, in particular, have been shown to reflect their robusticity and rigidity (Ruff and Hayes, 1983; Ruff et al., 1993). In a cross-sectional analysis of the Boxgrove tibia (Trinkaus et al., 1999), the authors noted some degree of deformation, which they corrected before deriving moments of area. However, although this method is suitable for nearly regular and concentric sections, the formulas they used to derive the moments of area have been suggested to potentially introduce errors when applied to other irregular and eccentric contours (Nagurka and Hayes, 1980; Ruff and Leo, 1986;

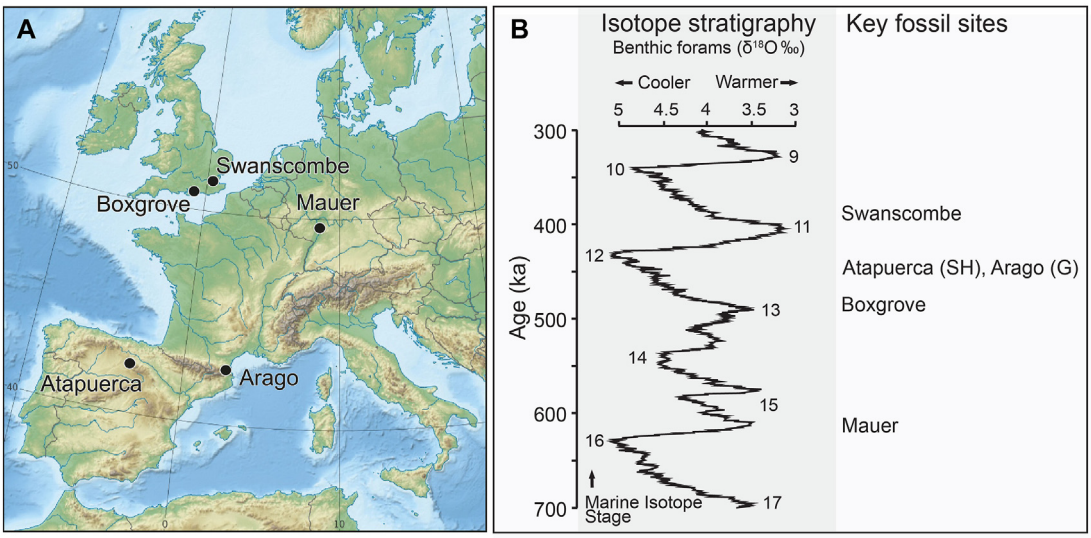

Figure 1. A) Location map and B) chronology of key European Middle Pleistocene hominin samples relative to the benthic foraminiferal oxygen isotopic stratigraphy (Lisiecki and Raymo, 2005).

Ohman, 1993). Thus, we present a new virtual reconstruction of the Boxgrove 1 tibia and a revised estimate of the cross-sectional parameters, allowing for a new morphological analysis of this specimen and comparison of the Boxgrove tibia with seven almost complete tibia specimens from SH.

In this article, we compare the dental and tibial morphology of two important and approximately contemporaneous MP hominin samples. The first aim is to assess whether the crown and root dental tissue proportions and root linear measurements of the two Boxgrove lower incisors, and the morphology and cross-sectional parameters of the Boxgrove tibia, fall within the variation of the SH population, or if these specimens more likely belong to another European paleodeme, or even to another species. The second aim is to compare the Boxgrove and SH assemblages to previously published literature on MP hominins to assess morphological diversity in the European MP fossil record more generally. This allows us to discuss the validity of assigning the Boxgrove and SH material to distinct paleodemes, and to consider their significance within the larger MP debate on the dynamics of human evolution in Europe.

1.1. Dating and archeology of Boxgrove

Boxgrove (West Sussex) is situated 50 m above sea level and about 10 km from the present-day coastline of the English Channel (Fig. 1A). The site was discovered in 1974, as a result of sand and gravel extraction in a quarry called Amey's Eartham Pit. Between 1974 and 1996, over 100 individual localities were excavated, and a high-resolution record of stone artifacts and fossilized mammal remains was recovered from a succession of buried land surfaces (Roberts and Parfitt, 1999). The quarrying exposed early MP interglacial marine deposits, an overlying paleosol, and associated freshwater pond deposits that were covered by colluvial and mass-movement sediments during the ensuing cold stage.

Human remains (a tibia and two mandibular incisors) were recovered from site Q1/B (Quarry 1, excavation area B), also colloquially known as either the 'Waterhole Site' or the 'Hominin Site' (Stringer et al., 1998; Hillson et al., 2010). The incisors are from the base of the freshwater deposits in an area that would have been dominated locally by freshwater pools formed by spring activity and wet grasslands backed to the north by a degrading cliff (Roberts and Pope, 2009). These deposits contain dense accumulations of well-made flint handaxes, flake tools, and debitage from their manufacture (Pope, 2002), intermingled with butchered large mammal remains (Roberts and Parfitt, 1999). The tibia was recovered from overlying deposits associated with a colluvial channel and gelifluction flow.

The interglacial deposits have been dated primarily based on mammalian biostratigraphy. The mammal fauna includes a combination of large and small mammals that went extinct at the end of early MP (e.g., *Stephanorhinus hundsheimensis*, *Praemegaceros* cf. *verticornis*, *Praemegaceros dawkinsi*, *Ursus deningeri*, *Pliomys episcopalis*) together with early forms of the living water vole (*Arvicola*) and narrowed-skulled vole (*Lasiopodomys gregalis*) that together characterize the latter part of the 'Cromerian Complex' correlated with MIS 13. The cold stage deposits are correlated with the major glacial period of MIS 12 (Fig. 1B; Preece and Parfitt, 2012). The Boxgrove hominin remains derive from deposits attributed to the cooling limb of the MIS 13 interglacial, at about 480 ka (Preece and Parfitt, 2012; Whittaker and Parfitt, 2017).

1.2. Dating and archeology of Sima de los Huesos

The Sima de los Huesos cave site is located within the deep chambers of the Sierra de Atapuerca karst system, a small range of hills near Burgos in northern Spain, covering about 12 square kilometers in area, and rising about 1000 m above sea level (Fig. 1; Arsuaga et al., 1997). It contains numerous karst cavities in Cretaceous limestone, many of which contain Pleistocene sediments. The first human remains at SH, associated with a large assemblage of cave bear (*U. deningeri*) fossils, were found in 1976, and the site has been under systematic excavation since 1984 (Aguirre et al., 1975; Aguirre and de Lumley, 1977). More than 6500 hominin remains from some 29 individuals have been found in the excavated deposits, concentrated in a single lithostratigraphic level (LU6) alongside carnivore fossils and speleothem intraclasts (Bermúdez de Castro et al., 2021). Analyses of the faunal assemblage suggested an early-to-mid MP age for the hominin-bearing layer (Cuenca-Bescós et al., 1997; García et al., 1997; Arsuaga et al., 2014),

which is consistent with recent chronological studies proposing an estimated age range between 427 ± 12 ka and 448 ± 15 ka for the SH hominins (Arnold et al., 2014; Arsuaga et al., 2014; Demuro et al., 2019). Uranium-series dating of a cave raft speleothem deposited directly on a hominin cranium from LU-6 yielded a mean age of 434 + 36/−24 ka (Arsuaga et al., 2014), whereas both single-grain TT-OSL ages for LU-5 and LU-6 and a Bayesian age-depth model built with published PIR-IR and TT-OSL chronologies from the level LU-6 provided a mean age of 448 ± 15 ka (Arnold et al., 2014; Demuro et al., 2019). These results allow the attribution of the SH hominin remains to early MIS 11 or, more probably, to late MIS 12 (Lisiecki and Raymo, 2005; Fig. 1B). In 1998, a large and apparently unused amygdaloid handaxe manufactured from a pinkish quartzite was recovered from the main hominin fossil-bearing deposits (Carbonell and Mosquera, 2006). It is the only artifact identified from SH so far (Bermúdez de Castro et al., 2004; Carbonell and Mosquera, 2006).

2. Materials and methods

2.1. Samples

Incisors The Boxgrove dental sample comprises two mandibular permanent incisors tentatively assigned to *H. heidelbergensis* (Hillson et al., 2010). Boxgrove 2 is a right lower central incisor (NHMUK PA EM 3567) exhibiting a wear grade 6 (Molnar, 1971); the detached tip of the root (NHMUK PA EM 3567b) was found nearby, in a bulk sample recovered approximately 1 m away from the main portion of the incisor (NHMUK PA EM 3567a; Hillson et al., 2010). Boxgrove 3 (NHMUK PA EM 3568) is a left lower lateral incisor with a wear grade 7 (Molnar, 1971). Both teeth have a large area of dentine exposed on the incisal surface surrounded by a thin enamel rim (Fig. 2). The wear pattern and context of the finds in the same level and in close proximity to each other suggest they belong to the same individual (Hillson et al., 2010).

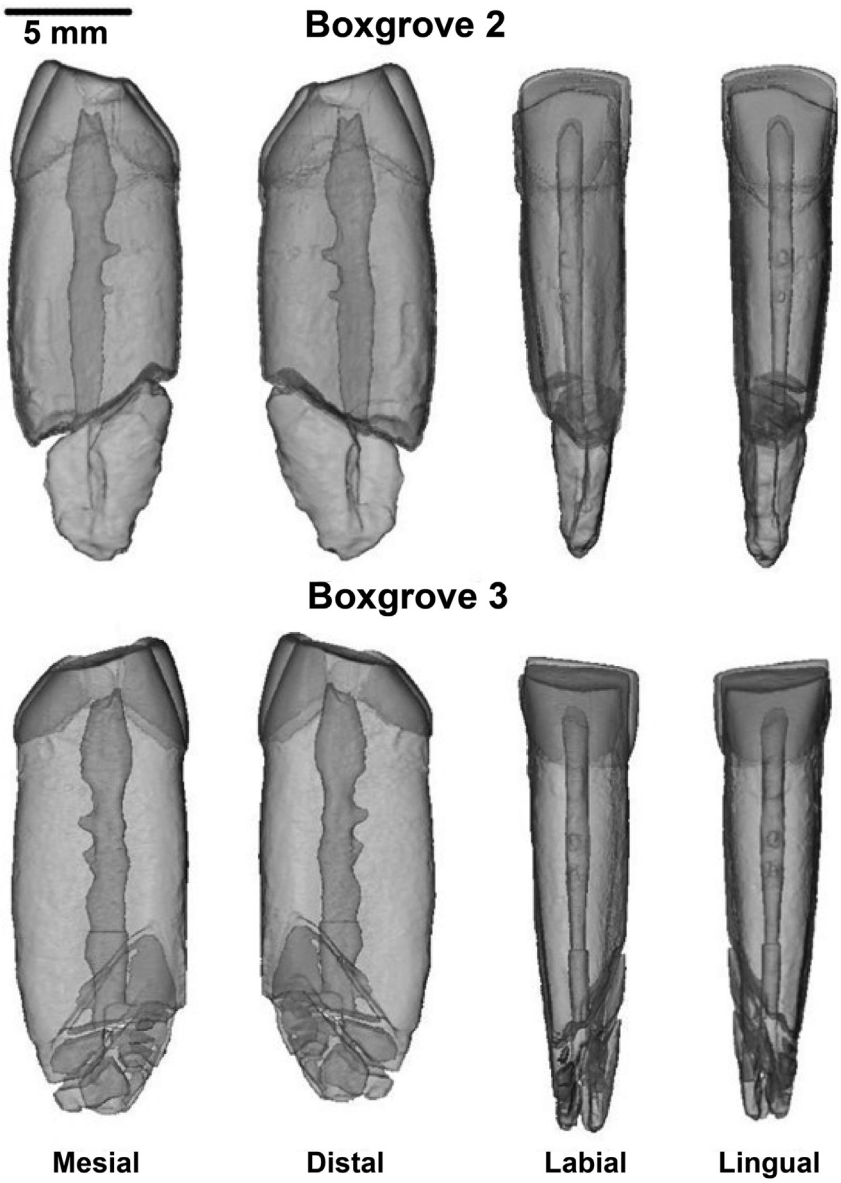

Figure 2. Three-dimensional models of Boxgrove 2 (right I_1: NHMUK PA EM M3567) and associated fragment (top) and Boxgrove 3 (left I_2: NHMUK PA EM M3568; bottom) made transparent to allow visualizations of the dental cavity.

Table 1
Sample composition of the central and lateral incisors, sample size, and sources of the comparative sample.

Sample	Number of teeth	Tooth type	Source
ATD	1	I_1	This study
	1	I_2	
SH	10	I_1	
	12	I_2	
Neanderthal (Krapina and Ehringsdorf)	4	I_1	
	5	I_2	
RMH (UCM)	23	I_1	
	17	I_2	
SH	6	I_1	Measured from published photographs
	5	I_2	(Martinón-Torres et al., 2012)
Tighennif	1	I_1	Zanolli and Mazurier (2013)
	1	I_2	
Atapuerca-Sima del Elefante (ATE9-1)	1	I_2	Prado-Simón et al. (2011)
Neanderthals (Las Palomas)	2	I_1	Walker et al. (2008); Bayle et al. (2017)
	2	I_2	
Neanderthals (Grotte du Portel Ariège)	1	I_1	Brabant and Sahly (1964)
Neolithic modern humans	13	I_2	Bayle et al. (2017)
RMH	13	I_2	
Multiple taxa (FMH, RMH, Neanderthals)	21	I_1	Smith et al. (2012)
	18	I_2	
Multiple taxa (FMH, RMH, Neanderthals, *H. erectus*, '*H. ergaster*', *H. heidelbergensis*, '*H. georgicus*')	74	I_1	Le Cabec et al. (2013)
	85	I_2	

Abbreviations: ATD = *H. antecessor*, Atapuerca – Gran Dolina; SH = Sima de los Huesos; RMH = recent modern humans; UCM = Universidad Complutense de Madrid; FMH = fossil modern humans.

The comparative dental material includes a total of 73 lower incisors belonging to Early and Middle Pleistocene hominins from Europe and a modern human sample (Tables 1 and 2): two incisors from Gran Dolina-TD6.2 (*Homo antecessor*; curated at the National Research Center on Human Evolution – CENIEH, Burgos, Spain), 22 from SH (curated at CENIEH), nine *Homo neanderthalensis* mandibular incisors from Krapina and Ehringsdorf (available on the open source information platform NESPOS; https://www.nespos.org), and 40 RMH specimens from the forensic collection of the Anatomical Department of Escuela de Medicina Legal de Madrid (curated at Universidad Complutense de Madrid, Spain; for a detailed description of this material see Lockey et al., Submitted for publication). We also included published measurements for 244 teeth for crown and root dental tissue proportions and dimensions (see Supplementary Online Material [SOM] Table S1 for details). These include incisors from Tighenif (Zanolli and Mazurier, 2013) dated to ca. 700 ka (Geraads et al., 1986), from Atapuerca-Sima del Elefante (ATE9-1; Prado-Simón et al., 2011) in level TE9 dated to ca. 1.2 Ma, from Neanderthals from Las Palomas dated to <43,000–40,000 cal BP (Walker et al., 2008; Bayle et al., 2017), and from Grotte du Portel in Ariège (Brabant and Sahly, 1964) dated to OIS 3–4 (Gardeisen, 1999). As part of these supplementary measurements, the SH sample was complemented with root length measurements taken by one of the authors (A.L.L.) from published photographs (Figs. 13 and 14 from Martinón-Torres et al., 2012) of 11 central and lateral incisors with complete roots. Published measurements for a sample of Neolithic and RMH from Bayle et al. (2017) were also included in the comparative data set, as well as 39 specimens from multiple taxa (fossil modern humans [FMH], RMH, Neanderthals) from Smith et al. (2012), and 159 specimens from multiple taxa (FMH, RMH, Neanderthals, *Homo erectus*, '*Homo ergaster*,' *H. heidelbergensis*, '*Homo georgicus*') from Le Cabec et al. (2013). The FMH sample comprises *Homo sapiens* specimens dated from MIS 2 and MIS 1.

Tibiae The hominin tibia discovered at Boxgrove in 1993 (Boxgrove 1—NHMUK PA EM 3566) is a left tibial shaft lacking its proximal and distal ends. It consisted of four major proximal fragments and two distal fragments before repairing the breaks (Roberts et al., 1994; Stringer et al., 1998; Trinkaus et al., 1999). Taphonomic modifications such as surface polish, incisions, grooves, and pits were observed, suggesting the impact of carnivore action, trampling, and/or pedoturbation on the preservation of the specimen (Stringer et al., 1998). Boxgrove 1 was excavated from a locality approximately 10 m from the Boxgrove 2 incisor and in a stratigraphically higher level, making it unlikely that the tibia and incisors originate from the same individual (Hillson et al., 2010). Boxgrove 1 presents a *Homo*-like tibial morphology, with features such as a diaphysis with rounded margins, mediolateral hypertrophy, a prominent tibial pilaster, and a relatively high level of diaphyseal robusticity (Roberts et al., 1994; Stringer et al., 1998; Trinkaus et al., 1999). Age-at-death could not be determined precisely for the Boxgrove 1 individual, with histomorphometric age estimates suggesting old age (Streeter et al., 2001) and ontogenetic growth pattern suggesting the specimen was a young adult (Gosman et al., 2013). It cannot be demonstrated that the Boxgrove postcranial and dental fossils represent a single population, but this is our working assumption in this article.

The comparative sample used for cross-sectional analysis was composed of seven complete tibiae from SH (from Rodríguez et al., 2018), 41 tibiae from RMH from the medieval cemetery at the San Pablo Monastery in Burgos (Spain), and Neanderthal, Early and Middle Upper Paleolithic (UP), and MP modern human (EMH) specimens drawn from Trinkaus and Ruff (2012; see SOM Table S1 in Rodríguez et al., 2018), and published data on the Broken Hill tibia (NHMUK PA EM 691; Trinkaus, 2009). The SH sample used for comparison had previously been analyzed by Arsuaga et al. (2015) and Rodríguez et al. (2018), highlighting morphological patterns similar to Neanderthal tibial specimens. These included rounder shaft sections than RMH, a relatively smaller medullar cavity, and very thick cortical bone along the shaft. For general shape comparisons, published data were used from Daka (Middle Awash, Ethiopia – BOU–VP-1/109; Gilbert, 2008), Broken Hill (Trinkaus, 2009), '*H. georgicus*' (Lordkipanidze et al., 2007), *Homo floresiensis* (Jungers et al., 2009), Neanderthals, and RMH.

Table 2
Composition of the original sample, including central and lateral incisors, analyzed in the study, with detailed information on the crown wear grade (following Molnar, 1971), root preservation (see footnote for a–d characterization), and analysis performed in each tooth.

Group	Accession number	Specimen code	Position	Side	Crown wear grade	Root preservation	Analysis
Boxgrove	NHMUK PA EM 3567	Boxgrove 2	Central	R	6	Incomplete[a]	All
Boxgrove	NHMUK PA EM 3568	Boxgrove 3	Lateral	L	7	Incomplete[a]	All
RMH (Modern, Spain)	UCM_8	–	Central	L	2	Complete	All
RMH (Modern, Spain)	UCM_9	–	Central	L	3	Complete	All
RMH (Modern, Spain)	UCM_14	–	Central	L	2	Complete	All
RMH (Modern, Spain)	UCM_15	–	Central	R	2	Complete	All
RMH (Modern, Spain)	UCM_16	–	Central	L	4	Complete	All
RMH (Modern, Spain)	UCM_19	–	Central	L	5	Complete	All
RMH (Modern, Spain)	UCM_21	–	Central	L	3	Complete	All
RMH (Modern, Spain)	UCM_30	–	Central	L	4	Complete	3D crown and root
RMH (Modern, Spain)	UCM_31	–	Central	L	3	Complete	All
RMH (Modern, Spain)	UCM_36	–	Central	L	3	Complete	All
RMH (Modern, Spain)	UCM_44	–	Central	L	3	Complete	All
RMH (Modern, Spain)	UCM_49	–	Central	L	3	Complete	All
RMH (Modern, Spain)	UCM_50	–	Central	L	2	Complete	All
RMH (Modern, Spain)	UCM_53	–	Central	L	4	Complete	3D crown and root
RMH (Modern, Spain)	UCM_54	–	Central	L	2	Complete	3D crown and root
RMH (Modern, Spain)	UCM_55	–	Central	L	2	Complete	All
RMH (Modern, Spain)	UCM_57	–	Central	L	2	Complete	All
RMH (Modern, Spain)	UCM_61	–	Central	L	2	Complete	All
RMH (Modern, Spain)	UCM_65	–	Central	L	2	Complete	All
RMH (Modern, Spain)	UCM_71	–	Central	R	4	Complete	All
RMH (Modern, Spain)	UCM_73	–	Central	L	3	Complete	All
RMH (Modern, Spain)	UCM_76	–	Central	L	2	Complete	All
RMH (Modern, Spain)	UCM_84	–	Central	L	4	Complete	3D crown and root
RMH (Modern, Spain)	UCM_8	–	Lateral	L	2	Complete	3D crown and root
RMH (Modern, Spain)	UCM_9	–	Lateral	L	4	Complete	All
RMH (Modern, Spain)	UCM_15	–	Lateral	R	4	Complete	All
RMH (Modern, Spain)	UCM_20	–	Lateral	L	2	Complete	All
RMH (Modern, Spain)	UCM_21	–	Lateral	L	2	Complete	All
RMH (Modern, Spain)	UCM_26	–	Lateral	L	2	Complete	All
RMH (Modern, Spain)	UCM_38	–	Lateral	L	2	Complete	All
RMH (Modern, Spain)	UCM_42	–	Lateral	L	3	Complete	All
RMH (Modern, Spain)	UCM_43	–	Lateral	L	3	Complete	All
RMH (Modern, Spain)	UCM_44	–	Lateral	L	3	Complete	All
RMH (Modern, Spain)	UCM_49	–	Lateral	L	5	Complete	All
RMH (Modern, Spain)	UCM_54	–	Lateral	L	3	Complete	All
RMH (Modern, Spain)	UCM_55	–	Lateral	L	1	Complete	All
RMH (Modern, Spain)	UCM_56	–	Lateral	L	4	Complete	All
RMH (Modern, Spain)	UCM_61	–	Lateral	L	2	Complete	All
RMH (Modern, Spain)	UCM_73	–	Lateral	L	4	Complete	All
RMH (Modern, Spain)	UCM_84	–	Lateral	L	4	Complete	All
Neanderthal	Ehringsdorf G1	G1	Central	R	2	Complete	All
Neanderthal	Krapina – D70	D70	Central	R	3	Complete	All
Neanderthal	Krapina – D72	D72	Central	L	5	Complete	All
Neanderthal	Krapina – D74	D74	Central	R	2	Incomplete[b]	2D and 3D crown
Neanderthal	Ehringsdorf G1	G1	Lateral	R	2	Complete	2D and 3D crown
Neanderthal	Krapina – D69	D69	Lateral	L	4	Complete	All
Neanderthal	Krapina – D71	D71	Lateral	R	3	Complete	All
Neanderthal	Krapina – D90	D90	Lateral	L	2	Incomplete[b]	2D and 3D crown
Neanderthal	Krapina – D198	D198	Lateral	R	4	Incomplete[b]	2D and 3D crown
SH	AT-104	3	Central	L	3	Incomplete[b]	All
SH	AT-555	7	Central	L	4	Complete	All
SH	AT-595	23	Central	R	4	Incomplete[b]	All
SH	AT-596	24	Central	R	3	Incomplete[c]	All
SH	AT-1742	2	Central	R	3	Incomplete[d]	All
SH	AT-1762	15	Central	L	4	Complete	All
SH	AT-2195	18	Central	L	3	Complete	All
SH	AT-2730	20	Central	L	3	Incomplete[d]	All
SH	AT-3253	28	Central	R	6	Complete	All
SH	AT-3882	25	Central	R	3	Complete	All
SH	AT-55	2	Lateral	R	3	Complete	All
SH	AT-103	3	Lateral	L	3	Incomplete[d]	All
SH	AT-167	11	Lateral	L	3	Incomplete[d]	All
SH	AT-195	7	Lateral	L	4	Complete	All
SH	AT-275	1	Lateral	R	3	Complete	All
SH	AT-594	23	Lateral	R	4	Complete	All
SH	AT-957	18	Lateral	R	3	Complete	All
SH	AT-1123	20	Lateral	R	3	Complete	All
SH	AT-1461	15	Lateral	R	4	Complete	All
SH	AT-2391	24	Lateral	L	3	Complete	All
SH	AT-2776	28	Lateral	L	6	Complete	All
SH	AT-3827	25	Lateral	R	3	Complete	All

Table 2 (*continued*)

Group	Accession number	Specimen code	Position	Side	Crown wear grade	Root preservation	Analysis
H. antecessor	ATD6-2	H1	Lateral	L	4	Complete	All
H. antecessor	ATD6-52	H5	Central	L	4	Incomplete[b]	2D crown and Root

Abbreviations: NHMUK = Natural History Museum, London (UK); RMH = recent modern humans; UCM = Universidad Complutense de Madrid; SH = Sima de los Huesos; AT = Atapuerca − Sima de los Huesos; ATD = Atapuerca − Gran Dolina; R = right; L = left.
[a] Root cracked or fractured for the lower third of the root. See Figure 2 models for visualization and Figure SOM S2 for reconstruction.
[b] 1/3 root missing and partly reconstructed.
[c] Minor damage to mid root labial side and partly reconstructed.
[d] Root tip broken and partly reconstructed.

2.2. Data collection

Incisors The Boxgrove incisors were scanned using microcomputed tomography (μCT) with the HMX-ST 225 CT System (Nikon Metrology, Tring, UK) housed at the Imaging and Analysis Centre, Core Research Laboratories, at the Natural History Museum (London, UK) (see SOM S1 for details about the scanning parameters used for each sample). The fossil teeth from Atapuerca TD6 and SH were scanned with the Scanco Medical AG Micro-Computed Tomography 80, at the Microscopy and Micro Tomography Laboratory at CENIEH (Burgos, Spain). The RMH sample (Universidad Complutense de Madrid) was scanned using an X-ray ICTP-ELETTRA MicroCT system at the Multidisciplinary Laboratory of the International Centre for Theoretical Physics (ICTP) in Trieste, Italy. The Neanderthal sample was sourced from NESPOS databases (Weniger et al., 2005). Image stacks were imported into Avizo v. 7 (Thermo Fisher Scientific, Waltham) to create 3D models that allow for a semiautomatic threshold-based segmentation and minor manual editing to separate the different dental tissues (enamel, dentine, and pulp cavity).

As all incisors, central and lateral, present extensive enamel wear (>3 stage following Molnar, 1971), no reliable nor comparable data on 2D and/or 3D crown measurements can be provided. However, future studies may compare data on specimens showing similar degree of wear across hominin species, and therefore we performed the 2D and 3D measurements to be included as supplementary material (see SOM Table S2 and SOM Fig. S1).

For 2D measurements, firstly, we followed the methodology outlined by Smith et al. (2012) to obtain the 2D mesial plane of section where linear measurements would be taken. Using Amira v. 6.3.0 (Thermo Fisher Scientific, Waltham, MA), the 3D model of the tooth was rotated to view the occlusal with the incisal edge set horizontally and the widest labiolingual diameter set vertically. Secondly, we located the central point of the incisal edge, and this point was set as the center of rotation. Finally, we created a 2D plane (slice) capturing the widest bicervical diameter resulting in the ideal plane of section. We used ImageJ v. 1.51 (Abràmoff et al., 2004) to measure the enamel and dentine (including pulp) areas (in mm^2), and the enamel–dentine junction (EDJ) length (in mm). Following Martin (1985), we calculated the average enamel thickness (AET = enamel area/EDJ length), the relative enamel thickness (RET = 100*AET/(dentine area1/2)), and the percentage of dentine and pulp in the molar crown (Acdp/Ac = 100*dentine area/total crown area in %; see SOM Table S2). For 3D measurements, we performed the segmentation of the dental tissues (enamel, dentine, and pulp) and assessed enamel volume thickness for the central and lateral incisors, using the Amira v. 6.3.0 semiautomatic tool, threshold-based segmentation, and manual correction. We used the protocol developed by Olejniczak et al. (2008) for the definition of the cervical plane; that is, the plane halfway between the most apical continuous ring of enamel and the plane containing the last hint of enamel. Following, we measured the volume of the enamel and dentine (including the pulp enclosed in the crown) in mm^3 and surface area of the EDJ (in mm^2). Finally, we calculated the 3D average enamel thickness (3D AET = enamel volume/surface area of the EDJ, in mm), 3D relative enamel thickness (3D RET = 100*3D AET/(dentine volume 1/3) a scale-free measurement), and the percentage of dentine and pulp in the total crown volume (Vcdp/Vc = 100*dentine volume/total crown volume in %; Kono, 2004; Olejniczak et al., 2008).

For root measurements, we divided the crown from the root at the cervical plane, following Le Cabec et al. (2013). Landmarks were set at the greatest curvature on labial and lingual sides of the cemento-enamel junction, and a best-fit plane was then computed (least squares criterion). We used the Avizo v. 7 (Thermo Fisher Scientific, Waltham, MA) 'volume edit tool' to measure the crown and root. For all incisor roots, both linear measurements and 3D volume data were extracted from well-preserved specimens and incisors that required reconstruction. The levels of damage for each tooth are reported in Table 2. When required, minimal reconstructions of the root apex followed the method of Zanolli et al. (2018) based on the 2−3D geometric approach. The virtual stack of images was first oriented with the buccal surface toward the x-axis. The data set was realigned to have the longitudinal sections passing along the root main axis. Then, the most apical transversal section that still displayed a complete root outline was defined as the reference root section. Perpendicular longitudinal sections were then positioned to pass through the center of the reference root section. In lateral views, the root apex was estimated on the longitudinal sections. This process was replicated on the perpendicular longitudinal section. Based on the two reconstructed perpendicular sections appearing as a cross on the reference root section, the broken root outline was reconstructed. The same process was repeated on more apical transversal sections until the last point of the reconstructed longitudinal sections was reached. Interpolations then were used between the reconstructed transversal slices to reconstruct the missing root volume (SOM Fig. S2).

We measured the root variables following Le Cabec et al. (2013): maximum labiolingual crown diameter (CrLL, in mm); labiolingual cervical root diameter (RLL, in mm); mesiodistal cervical root diameter (RMD, in mm); cervical area (CA, mm^2); root length (RL, in mm); radicular dentine volume (RDV, mm^3); root pulp volume (RPV, mm^3); and total root volume (RV, mm^3; Table 3).

Tibiae Tomographic scanning of the Boxgrove tibia was carried out at the Imaging and Analysis Centre, Core Research Laboratories, at the Natural History Museum (London, UK), with an HMX-ST 225 CT System (Nikon Metrology, Tring, UK). Cross-sectional images of Boxgrove 1 were obtained in two different pieces, the distal and proximal shaft fragments (see SOM S1 for detail about the scanning parameters used for each sample). Tomographic scanning of the SH hominins and RMH specimens was performed at the University of Burgos (Spain), with a YXLON Compact X-Ray industrial multislice CT scanner. The CT images were visualized using the software package Mimics (Materialise NV, Belgium).

To assess tibial cross-sectional shape and thickness and, in turn, evaluate tibial robusticity and rigidity, a set of cross-sectional

Table 3
Descriptive statistics for root tissue proportions for the central and lateral mandibular incisor for Boxgrove and comparative material.

Crown and root for Boxgrove									
Boxgrove	Specimen	Labiolingual crown diameter (mm)	Labiolingual cervical root diameter (mm)	Mesiodistal cervical root diameter (mm)	Cervical area (mm^2)	Root length (mm)	Root dentine volume (mm^3)	Root pulp volume (mm^3)	Total root volume (mm^3)
NHMUK PA EM 3567	Original	7.29	6.76	4	21.23	10.85	191.42	9.84	201.26
NHMUK PA EM 3568	Original	7.34	6.9	4.25	23.02	14.87	242.07	8.73	250.8
NHMUK PA EM 3567	Reconstruction	–	–	–	–	14.94	210.18	9.83	220.11
NHMUK PA EM 3568	Reconstruction	–	–	–	–	15.21	239.17	10.12	259.29
Mandibular central incisors for the comparative sample									
Sample		Labiolingual crown diameter (mm)	Labiolingual cervical root diameter (mm)	Mesiodistal cervical root diameter (mm)	Cervical area (mm^2)	Root length (mm)	Root dentine volume (mm^3)	Root pulp volume (mm^3)	Total root volume (mm^3)
RMH	Mean	5.69	5.57	3.31	14.49	12.76	117.21	4.07	121.28
	SD	0.42	0.44	0.25	1.90	1.62	28.21	1.70	29.21
	Minimum	5.14	4.95	2.93	12.01	9.50	70.95	0.99	75.03
	Maximum	6.77	6.63	3.99	19.36	16.11	176.94	8.05	182.48
Neanderthal	Mean	7.53	7.39	4.59	26.84	17.38	308.28	20.16	328.44
	SD	0.9	1.03	0.41	5.91	1.88	44.23	1.63	45.48
	Minimum	6.49	6.21	4.13	20.13	15.64	258.78	19.08	277.86
	Maximum	8.07	8.09	4.92	31.25	19.38	343.91	22.04	365.95
SH	Mean	6.45	6.31	3.85	19.06	16.47	219.31	14.96	234.27
	SD	0.31	0.28	0.21	1.65	1.26	26.91	5.97	25.67
	Minimum	6.13	6.04	3.59	17.87	13.77	191.06	7.28	210.85
	Maximum	7.10	6.90	4.35	23.56	18.36	285.86	26.71	297.17
ATD		7.59	7.48	4.06	30.37	17.05	359.89	17.05	376.94
Mandibular lateral incisors for the comparative sample									
Sample		Labiolingual crown diameter (mm)	Labiolingual cervical root diameter (mm)	Mesiodistal cervical root diameter (mm)	Cervical area (mm^2)	Root length (mm)	Root dentine volume (mm^3)	Root pulp volume (mm^3)	Total root volume (mm^3)
RMH	Mean	5.90	5.73	3.62	16.21	14.12	143.11	4.65	147.76
	SD	0.43	0.49	0.34	2.64	1.97	33.54	1.84	34.56
	Minimum	5.10	4.95	2.87	12.75	10.92	92.28	2.22	97.11
	Maximum	6.83	6.81	4.37	21.65	17.08	198.36	9.88	202.37
Neanderthal	Mean	8.5	7.92	5.56	34.54	17.65	432.63	25.42	458.04
	SD	0.44	0.03	0.02	0	0.74	30.67	0.12	30.79
	Minimum	8.19	7.9	5.54	34.54	17.13	410.94	25.33	436.27
	Maximum	8.81	7.94	5.57	34.54	18.17	454.31	25.5	479.81
SH	Mean	7.12	6.90	4.45	24.13	17.53	293.74	23.94	317.68
	SD	0.39	0.42	0.31	2.47	1.10	48.46	9.21	51.02
	Minimum	6.39	6.20	3.94	20.62	15.37	224.12	9.62	242.98
	Maximum	7.74	7.63	5.05	29.45	19.02	388.78	37.66	417.31
ATD			7.20	3.30	30.37	17.40	305.33	17.40	322.73

Abbreviations: RMH = recent modern humans; NHMUK = Natural History Museum, London (UK); SH = Sima de los Huesos; ATD = *H. antecessor*, Atapuerca – Gran Dolina.

parameters was measured on the specimens: total subperiosteal area (TA); cortical subperiosteal area (CA, a measure of resistance to axial loads, Ruff et al., 1993); maximum (Imax), and minimum (Imin) second moments of area (to assess bending rigidity in the reference planes); polar second moment of area (J, an indication of resistance to torsion and a general reflection of overall rigidity); and section moduli at bone midshaft (to measure the bending and torsional strength; where Zp represents the cross-sectional torsional strength). Because of the difficulties in orienting incomplete specimens with confidence, only TA and CA, Imax, Imin, and J, were considered for the analysis of Boxgrove 1. Cortical area relative to TA (%CA) was used as a proxy for diaphyseal robusticity. Diaphyseal shape was examined using Imax and Imin.

2.3. Data analyses

Incisors For comparative analysis of the incisors, and due to having only two incisors from Boxgrove, we used the adjusted (or modified) Z-score, which allows for comparison between small and unbalanced samples using Student's inverse t distribution. In these Z-scores, the −1.0 to +1.0 interval comprises 95% of the variation in the reference sample (Maureille et al., 2001; Scolan et al., 2012). Adjusted Z-scores were conducted on CA, RL, and RV (variables that captured the overall morphology) for the Boxgrove specimen, computed on the means and standard deviations of the Neanderthals and RMH groups. Qualitative assessment was conducted for all major root variables.

As both Boxgrove incisor roots required reconstruction, an interobserver error test was conducted by two of the authors (A.L.L and L.M.-F.) and Clément Zanolli. For total root volume, Boxgrove 2 had <1% difference, and Boxgrove 3 <2% difference (SOM Table S3). Considering these low values, which are lower than the reported 4% threshold error (e.g., Zanolli et al., 2010, 2018), our estimates from reconstructed roots therefore appear accurate. Because of the extensive crown wear, we provide descriptive statistics for the crown (SOM Table S2) and a more in-depth analysis of the roots.

Tibiae To compare the robusticity pattern of the tibiae among the different groups or paleodemes used in this analysis, tibial diaphyseal strength should be assessed relative to the baseline loads placed upon it, with body mass being the main load that models bone shape during growth (Ruff et al., 1993). Taking into consideration tibial sample size limitations for scaling to bone length and body mass, it is preferable (if possible) to carry out a standardization of J by the biomechanical length of the bone as a proxy for body size (Ruff et al., 1993). As Boxgrove 1 is missing both epiphyses, we performed a virtual reconstruction using Mimics to estimate its biomechanical length and, in turn, estimate the individual's stature. For this, the different specimens (SH and RMH) were assessed to identify the specimen whose mid-diaphysis external robusticity was closest to that of Boxgrove. This individual was SH Tib-XII. The anteroposterior (AP) mid-diaphysis in Boxgrove is free of distortion, with an AP diameter of 39 mm (Stringer et al., 1998). In comparison, the AP diameter of Tib-XII is 37.48 mm. Assuming the AP diameter vs. length proportions are similar in these two specimens, Tib-XII was scaled (enlarged) by 1.04 to estimate a probable articular length for the Boxgrove tibia. We then located and fixed the diaphyseal foramen and the midshaft in the Boxgrove specimen with that of the scaled Tib-XII tibia.

For cross-sectional analyses, sections at 20%, 35%, 50%, 65%, and 80% of tibial biomechanical length levels were chosen following Ruff and Hayes (1983) and Trinkaus and Ruff (2012). The analyses were performed using Moment-Macro (https://www.hopkinsmedicine.org/fae/mmacro.html) in ImageJ v. 1.53k (Abràmoff et al., 2004). Because the proximal and distal fragments that constitute Boxgrove 1 did not fit perfectly, with a narrower section in the refitted proximal portion compared to the distal portion, the four largest pieces of the proximal fragment were virtually separated before analysis to allow a reconstruction of the proximal shaft and obtain new results for the 65% and 80% cross-sections (Fig. 3). Three different cross-sectional reconstruction approaches were tested to establish the most plausible one: 1) Boxgrove 1 physically reconstructed (PR) without virtual reconstruction; 2) two-dimensional reconstruction (2DR) of cross-section images fixing the edges; and 3) three-

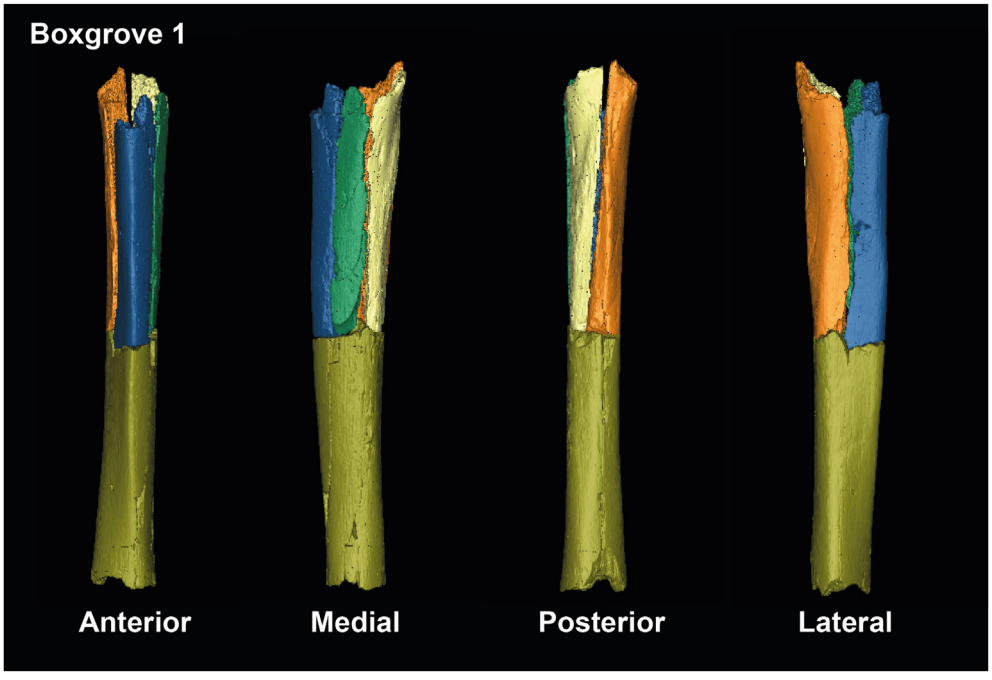

Figure 3. Boxgrove 1 (NHMUK PA EM 3566) reconstruction with anterior, medial, posterior, and lateral views.

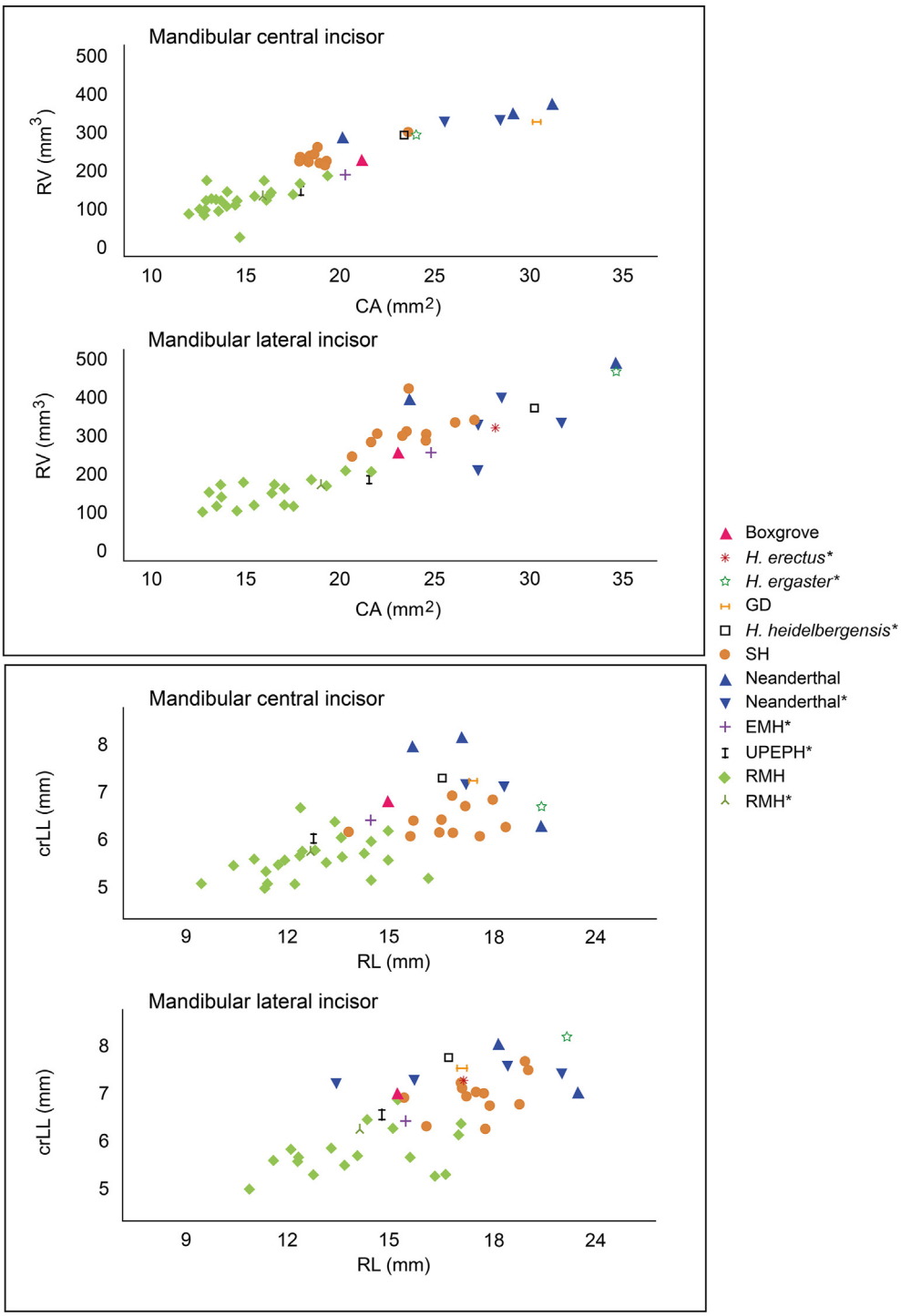

Figure 4. Bivariate scatter plots of total root volume (RV) vs. cervical area (CA) for I_1 and I_2 (top) and root length (RL) vs. labiolingual cervical diameter (crLL) for I_1 and I_2 (bottom). Samples include previously unpublished data from Boxgrove, Gran Dolina-TD6 (GD), Sima de los Huesos (SH), *H. neanderthalensis*, recent modern humans (RMH), and samples plotted from published sources (Le Cabec et al., 2013: *H. erectus* [S7_50], '*H. ergaster*' [KNW-WT 1500], *H. heidelbergensis* [Mauer]), and large samples representing Neanderthals, MP modern humans (EMH; Qafzeh and Skhul), Upper Paleolithic and Epipaleolithic modern humans (UPEPH), and RMH. All literature extracted from published material is indicated with an asterisk (*). (For interpretation of the references to color in this figure legend, the reader is referred to the Web version of this article.)

dimensional virtual reconstruction (3DR) of the Boxgrove 1 tibia following tibia distal diaphysis shape.

To provide a synthetic functional image through a visual representation of topographic thickness variation among Boxgrove, SH, and RMH, we performed a thickness analysis with Materialise 3-matic Medical (Materialise NV, Belgium). This software allows detection of differences in cortical thickness in absolute values in each specimen, so the differences in thickness of each bone are standardized by assigning an individual color scale—with minimum (green) and maximum thickness (red) values as the extremes of variation and yellow the mean value—that we can compare between individuals.

We also revisited the morphology and size of the Boxgrove 1 tibia to determine the affinities with those from the MP fossil

record. For this assessment, we compared Boxgrove with the specimens selected from published literature (see Section 2.1.), the seven nearly complete tibia specimens from SH, and the 41 RMH specimens that were used in order to be the model for the morphological comparison of Boxgrove 1 general external shape. Recent modern humans have different diaphyseal proportions compared to Neanderthals and SH specimens, being much less robust; for example, an RMH with an articular length of 370 mm will yield a diaphyseal diameter of ~31 mm; Boxgrove is therefore 1.25 times more robust. Thus, to fit biomechanical length with diaphyseal dimensions, we chose an RMH specimen with that biomechanical length, scaling its diaphyseal diameters to that of Boxgrove 1.

To compare the Boxgrove 1 tibia with those of SH, RMH, and fossil samples from the literature (Trinkaus and Ruff, 2012), the %CA and Imax/Imin indices were calculated. The combination of CA and TA reflects the differential subperiosteal deposition and endosteal resorption of bone, principally during development (Trinkaus and Ruff, 2012). The Imax/Imin index reflects the general shape of the section in which values close to one have more circular sections, whereas values greater than one have oval sections, in which there is one shaft that supports much more load than another.

The polar second moment of area (J) provides both an indication of resistance to torsion and a general reflection of overall rigidity. As indicated earlier, J should be standardized by an estimate of body mass. Given the scarcity of tibial MP fossil remains and the absence of associated pelvic or femur remains with which to calculate body mass, it is preferable to use biomechanical tibial length, which we obtained from the virtual reconstruction as explained earlier. With those data, we performed a reduced major axis (RMA) regression of the natural logarithm of J vs. biomechanical tibial length, using RMH and UP specimens for the comparison. We chose to use RMA because our aim is to summarize the relationship between two variables rather than to generate a predictive model. Logarithm transformation of J and biomechanical tibial length was performed to minimize regression bias (Ruff, 1995). In addition, stature was calculated using the Sjøvold (1990) formula, as used by Carretero et al. (2012) for SH and Neanderthal populations. The formula used in this article for the tibial material was as follows:

$$\text{Stature} = 3.29 \times \text{TL} + 47.34 \pm 4.15$$

where, TL is the total length from the top of the lateral proximal condyle to the tip of the distal malleolus (proximal spines are not included), as defined by Martin and Saller (1957) in which TL is referred to as M1.

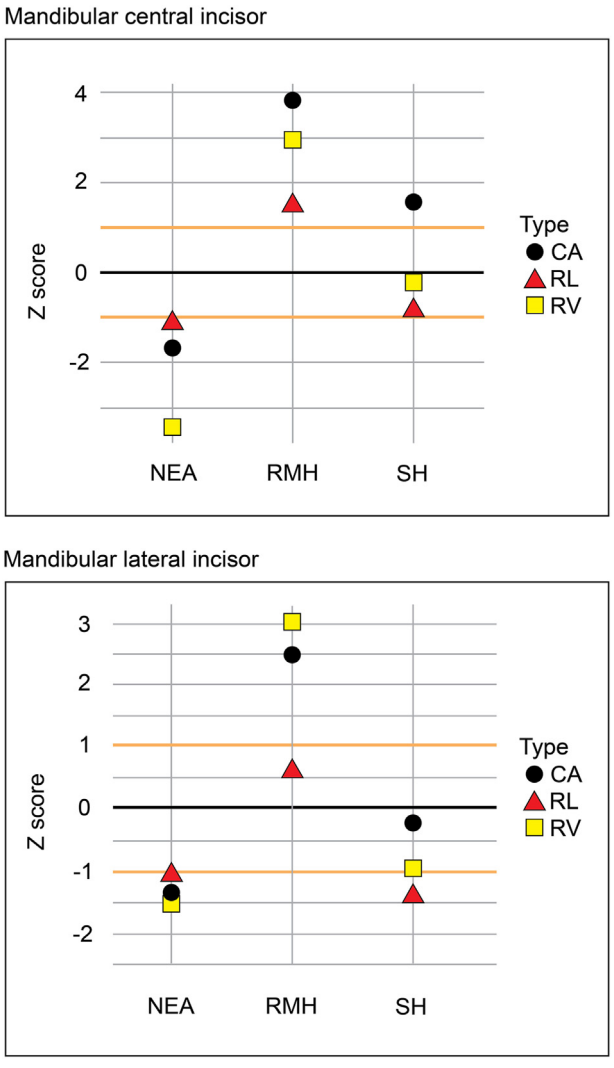

Figure 5. Adjusted Z-score of the root variables cervical area (CA), root length (RL), and root volume (RV) for the mandibular incisors from Boxgrove 2 (right I_1: NHMUK PA EM 3567) (top) and Boxgrove 3 (left I_2: NHMUK PA EM 3568; bottom) and compared to the variation expressed by Neanderthals (NEA), recent modern humans (RMH), and Sima de los Huesos (SH). The solid black line passing through zero represents the mean, and the yellow lines correspond to the estimated 95% limit of variation expressed for the comparative samples. (For interpretation of the references to color in this figure legend, the reader is referred to the Web version of this article.)

3. Results

3.1. Endostructural analysis of the Boxgrove mandibular incisors

Table 3 shows the descriptive measurements for the Boxgrove incisors and the comparative samples. Figure 4 shows the position of Boxgrove in relation to the comparative sample for CA relative to RV, and CrLL relative to RL. Boxgrove has a ratio of CA to RV similar to SH, as well as to EMH. Boxgrove has larger CA and RV compared to *H. sapiens*. The Boxgrove CA and RV are otherwise reduced relative to other extinct hominins. Boxgrove 2 and 3 have wide CrLL relative to RL compared to RMH, falling close to SH. Boxgrove and SH have smaller CrLL relative to RL in comparison to other extinct hominins. Boxgrove teeth share an intermediate position for RL and RV with SH, with longer and larger roots than RMH but shorter and smaller relative to other extinct hominins (*H. erectus*, '*H. ergaster*,' *H. antecessor* from Gran Dolina-TD6.2, *H. heidelbergensis* from Mauer, Neanderthals; Fig. 4; SOM Fig. S3) and the RV value of the Sima del Elefante I_2 (336.42 mm^3 taken from Prado-Simón et al., 2011). For the adjusted Z-scores (Fig. 5; Table 4), Boxgrove 2 falls within the 95% limit of variation (confidence interval) of SH for RV and RL. Boxgrove 3 falls within the 95% limit of variation for SH CA and RV and RMH for RL. For other variables, Boxgrove 2 and 3 fall outside of the 95% limit of variation compared to Neanderthals, SH, or RMH. Overall, for root traits, the Boxgrove incisors show the greatest affinities with the SH specimens, although there is overlap among groups.

Owing to the severe crown wear of the Boxgrove incisors, we were unable to extract meaningful results, and no taxonomic signal was identified in the surviving parts of the crowns.

3.2. Morphological and cross-sectional analyses of the Boxgrove tibia

Boxgrove 1 is similar in diaphyseal proportions to the SH Tib-XII complete tibia (Fig. 6A; Table 5). Using Tib-XII as a model, virtual

Table 4
Adjusted Z-scores for root length of Boxgrove mandibular incisors: Cervical area and root volume relative to recent modern humans, Neanderthals, and Sima de los Huesos.

Mandibular central incisors: Boxgrove 2 (NHMUK PA EM 3567)			
Index	Cervical area	Root length	Root volume
RMH	3.84	1.51	2.93
Neanderthals	−1.68	−1.13	−3.43
SH	1.56	−0.85	−0.21
Mandibular lateral incisors: Boxgrove 3 (NHMUK PA EM 3568)			
Index	Cervical area	Root length	Root volume
RMH	2.49	0.60	3.01
Neanderthals	−1.34	−1.06	−1.53
SH	−0.21	−1.42	−0.98

Abbreviations: RMH = recent modern humans; SH = Sima de los Huesos.

reconstruction of the Boxgrove tibia results in a biomechanical length of 370 mm, which is consistent with the lower estimate of Stringer et al. (1998). Based on this estimate, stature was calculated, providing an estimate of 177.3 ± 4.15 cm for the stature of the Boxgrove individual. External measurements of Boxgrove 1 show that this specimen is the largest compared to all other studied samples (Table 5).

With respect to shape, Boxgrove 1 is shown to have a more angular cross-section and its posterior face is flatter than in Neanderthals and SH, which are characterized by a section with an oval or amygdaloid morphology. In comparison, Daka (Middle Awash, Ethiopia: BOU-VP-1/109; Gilbert, 2008), Broken Hill (Trinkaus, 2009), '*H. georgicus*' (Lordkipanidze et al., 2007), and *H. floresiensis* (Jungers et al., 2009) share the straight and more angulated morphology observed in Boxgrove 1, in contrast to the patterns observed in SH and Neanderthal specimens. When using a modern human tibia with a biomechanical length of 370 mm as a model for Boxgrove 1, and a scaled diameter of 1.24, the Boxgrove tibia fits the shape of the modern human tibia almost perfectly (Fig. 6B), and presents a rounded and straight anterior border, as well as a flatter posterior surface than SH (See SI in Rodríguez et al., 2018).

Cross-sectional analysis When comparing the results from the present cross-sectional analysis (Table 6; Fig. 7) with those of Trinkaus et al. (1999), similar values were obtained for the distal fragment, but values diverge for the reconstructed proximal fragment. The two fragments differ in shape, with the distal portion having a less circular section than the proximal fragment, as expected. Two-dimensional reconstruction of cross-section images, fixing the fissures of the bone, and physical reconstructions fail because of the proximal fragment being narrower than expected for a human specimen, as noted by Trinkaus et al. (1999). The 3D-reconstructed tibia sections of Boxgrove 1 shown in Table 6 are most similar to those reported by Trinkaus et al. (1999).

When comparing the values obtained for TA, CA, Imax, Imin, J, %CA, and Imax/Imin for Boxgrove 1 with those of Neanderthals and SH, there are more similarities with *H. neanderthalensis* and SH than with Broken Hill or RMH (Table 7; Figs. 8 and 9). Regarding cross-section cortical thickness %CA (Fig. 8), Boxgrove 1 and other fossil humans have a relatively higher %CA and thicker bone cortices than RMH. Boxgrove 1 shares a similar distribution pattern with Broken Hill and Neanderthals, the 50% section having the thickest cortex. Boxgrove falls within the SH variability except at the 20% and 35% sections, where Boxgrove displays narrower cortices. This pattern is similar to that of Broken Hill, although this individual is thicker at every level. Regarding Imax/Imin (Fig. 9), Boxgrove 1 shares a similar pattern with Neanderthals, SH, and MP modern humans (EMH), and differs from RMH and Broken Hill.

With respect to bone robusticity, the Boxgrove tibia is shown to be the most robust among all the comparative samples, at all section levels (Fig. 10). In the original article (Trinkaus et al., 1999), the authors calculated Z-scores relative to EMH for the comparison of the 50% LJ relative to the 35% LJ, and established that Boxgrove fits better with the Neanderthal tibial model than with UP modern humans, although the difference in shape was not significant. To validate this former analysis, the LJ values relative to biomechanical length were compared using an RMA analysis in which the reference line was that calculated for anatomically modern humans (i.e., RMH and UP specimens). Results show that Boxgrove plots above the regression line of anatomically modern humans, similarly to Neanderthal and the SH samples.

Wall thickness analysis The anterior crest, soleal line, and tibia pilaster are the thickest parts of the Boxgrove 1 tibia (Fig. 11A). In Figure 11B, we observe a pattern more typical of RMH, where the greatest thickness is located in the tibial spine at midshaft, and is independent of wall thickness. Figure 11 illustrates the high relative thickness of the soleal line and tibial spine. Boxgrove 1 appears more similar to Tib-XII in terms of wall thickness, than to RMH (Fig. 11).

4. Discussion

4.1. High morphological variability in mandibular incisors: Evidence against the existence of distinct paleodemes in Europe during the Middle Pleistocene?

For extinct and extant late *Homo*, mandibular incisor morphology is extremely similar, except for a generally larger size in Neanderthals relative to RMH (Bailey, 2006). Compared to molars (Olejniczak et al., 2008; Skinner et al., 2015; Martín-Francés et al., 2018, 2020; Lockey et al., 2020) incisors are less taxonomically discriminative. As shown in previous studies (Lockey et al., 2020), we found that extreme wear also reduces the utility of crown dental tissue proportions for classification purposes.

The morphology of the roots firmly places Boxgrove within the range of variation of the SH sample. In all root traits, the Boxgrove incisors show greater robusticity than those in the RMH sample. Both SH and Boxgrove are within or below the lower ranges of other MP hominins for RL and RV, with slightly less robust roots. The pulp cavities of the Boxgrove incisors have mesiodistally flattened radicular canals (Fig. 2); this interpretation is limited, however, by excess deposition of secondary dentine and the impact of excessive wear altering the pulp cavity morphology in both teeth. This radicular pulp cavity morphology conforms to the shape of the LI_2 from Sima del Elefante, Spain (Prado-Simón et al., 2011) and the lower incisors from the Neanderthal individual from Regourdou, France (Macchiarelli et al., 2013). This radicular pulp cavity does, however, differ from the Tighenif mandibular incisors, which are reported as having an ovoid cross-section (Zanolli and Mazurier, 2013). The limited amount of comparative μCT material for

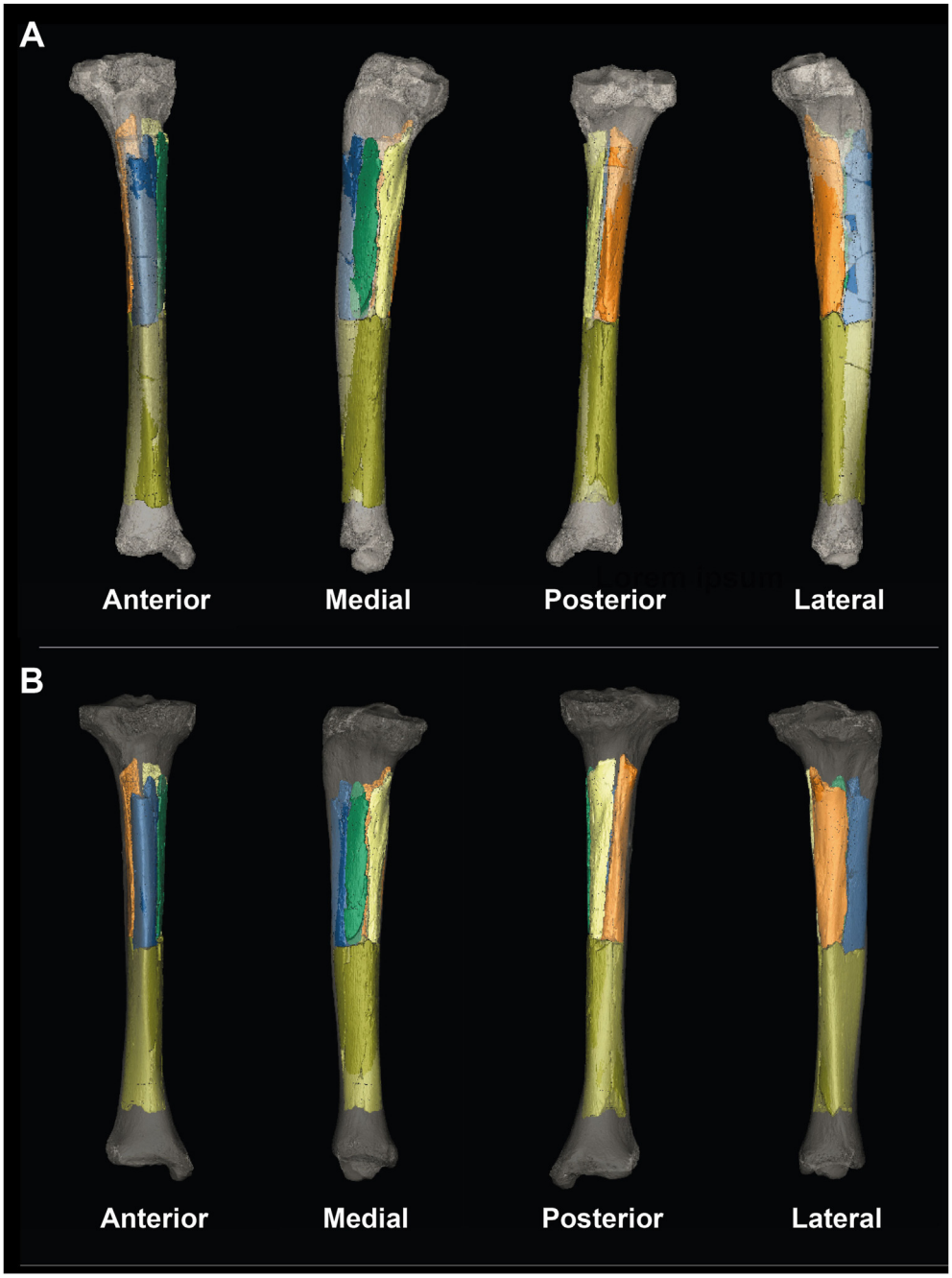

Figure 6. Boxgrove 1 (NHMUK PA EM 3566) reconstruction overlaying reconstructions of A) SH Tib-XII and B) modern human (scaled 1.25x only in anteroposterior and mediolateral diameters). Anterior, medial, posterior, and lateral views.

Table 5
External measurements for Boxgrove 1 tibia (NHMUK PA EM 3566) and means ± standard deviations (sample sizes in parentheses) for the comparative samples. All measurements in mm.[a]

	Boxgrove 1		SH	Neanderthal	RMH
	Original reconstruction	3D reconstruction			
Proximal AP diameter	44.63	46.55	41.35 ± 2.8 (6)	37.9 ± 3.4 (11)	31.34 ± 3.43 (198)
Proximal ML diameter	30.95	32.51	27.12 ± 2.21 (6)	26.4 ± 1.8 (11)	24.40 ± 2.36 (199)
Midshaft AP diameter	39.1	39.1	33.62 ± 4.01 (7)	31.6 ± 4.2 (11)	27.12 ± 3.30 (196)
Midshaft ML diameter	27.5	27.5	23.47 ± 1.67 (7)	22.5 ± 1.7 (11)	22.47 ± 3.83 (197)

Abbreviations: SH = Sima de los Huesos; RMH = recent modern humans; AP = anteroposterior; ML = mediolateral.
[a] Sources: RMH (San Pablo monastery), this paper; SH individuals, this paper and Arsuaga et al. (2015).

Table 6
Cross-sectional analysis of geometric parameters of the Boxgrove 1 tibia (NHMUK PA EM 3566).

Section	TA (mm^2)	CA (mm^2)	%CA	Imax (mm^4)	Imin (mm^4)	Imax/Imin	J (mm^4)	Zp (mm^3)
20	798.87	323.95	40.55	34544.7	31778.3	1.09	66323.0	3686.1
35	706.58	506.73	71.72	44576.4	30702.7	1.45	75279.0	4218.3
50	776.85	601.75	77.46	67628.0	32432.2	2.09	100060.2	4786.9
65 PR[a]	799.25	522.72	65.4	73711.4	28421.1	2.59	102132.5	4628.9
80 PR[a]	993.73	477.79	48.08	94006.2	35913.9	2.62	129920.2	5348.1
65 2DR[b]	726.81	465.37	64.03	61344.0	22432.3	2.73	83776.3	4005.2
80 2DR[b]	859.47	423.75	49.3	68630.9	24832.9	2.76	93463.8	4274.5
65 3DR[c]	869.03	587.55	67.61	86278.1	35264.5	2.45	121542.6	5385.8
80 3DR[c]	1025.8	490.55	49.72	107724.6	42078.9	2.56	149803.5	6100.7

Abbreviations: TA = total area; CA = cortical area; Imax = second moments of area—maximum; Imin = second moments of area—minimum; J = polar moment of area; Zp = cross-sectional torsional strength.
[a] PR, cross sectional parameters of Boxgrove 1 physically reconstructed without being virtually reconstructed.
[b] 2DR, cross sectional parameters of 2D reconstruction of cross-section images, fixing the fissures of the bone.
[c] 3DR, cross sectional parameters of 3D virtual reconstruction of the Boxgrove 1 tibia proposed in this paper.

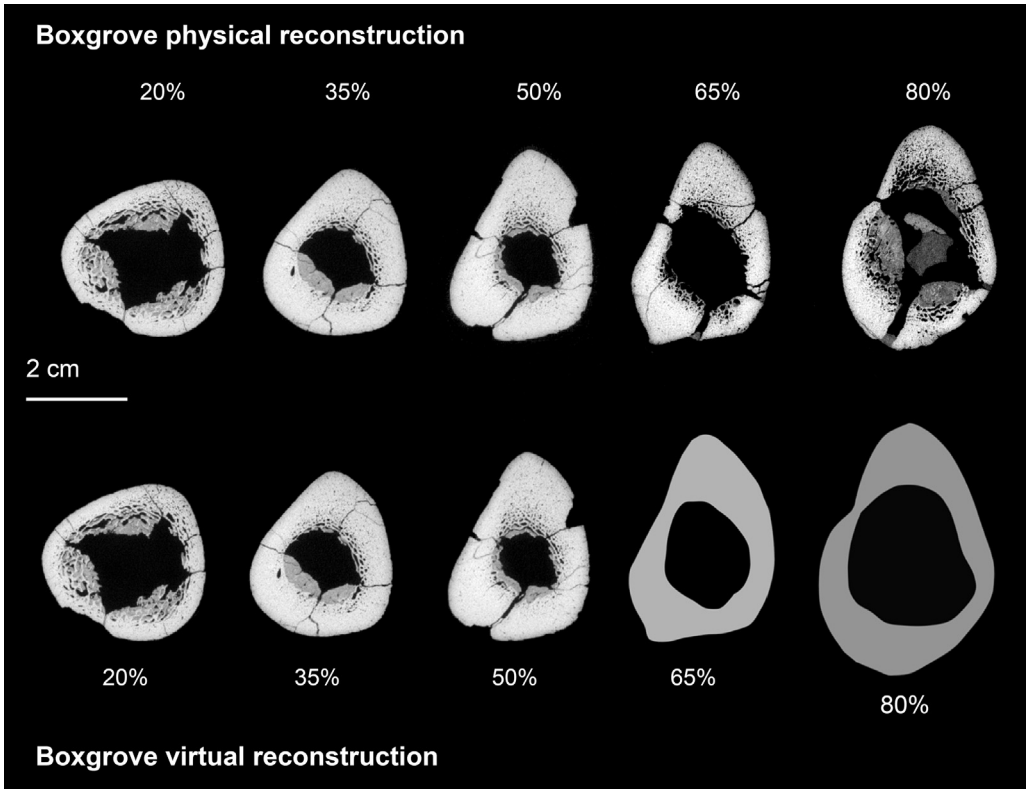

Figure 7. Boxgrove 1 cross-section images, original and virtual reconstruction, with percentages reflecting the position of the cross-section along the shaft.

Table 7
Comparison sample for geometric parameters. Fossil sample from Trinkaus and Ruff (2012), recent modern humans and Sima de los Huesos samples from the current study and Rodriguez et al. (2018).

			TA	CA	%CA	Imax	Imin	Imax/Imin	J
20%	Neanderthals	Mean	501.50	261.38	0.52	18573.50	13373.88	1.41	31947.38
		SD	71.75	53.85	0.09	5699.34	3716.30	0.32	8629.59
		n	8	8	8	8	8	8	8
	EMH	Mean	530.00	282.33	0.54	20202.00	15447.67	1.31	35649.67
		SD	34.04	18.77	0.06	1829.01	518.76	0.08	2344.17
		n	3	3	3	3	3	3	3
	UP	Mean	434.71	244.53	0.57	14827.53	10787.41	1.37	25614.94
		SD	94.07	46.48	0.09	6225.46	4226.08	0.22	10263.10
		n	17	17	17	17	17	17	17
	RMH	Mean	391.30	170.36	0.44	9482.19	7507.34	1.56	16989.52

Table 7 (*continued*)

			TA	CA	%CA	Imax	Imin	Imax/Imin	J
		SD	71.58	38.02	0.08	3062.65	3212.75	1.75	5909.51
		n	41	41	41	41	41	41	41
	SH	Mean	518.88	293.73	0.57	19135.28	16429.68	1.16	35564.97
		SD	64.28	40.80	0.06	5091.47	3357.57	0.10	8364.05
		n	6	6	6	6	6	6	6
35%	Neanderthals	Mean	488.56	364.11	0.74	24896.22	13931.78	1.75	38828.00
		SD	91.34	80.74	0.04	10367.76	4707.91	0.34	14764.35
		n	9	9	9	9	9	9	9
	EMH	Mean	568.00	418.00	0.74	31520.50	18435.50	1.73	49956.00
		SD	47.22	9.88	0.06	3524.17	3106.01	0.21	5882.27
		n	6	6	6	6	6	6	6
	UP	Mean	400.59	301.95	0.75	18965.82	8740.91	2.15	27706.73
		SD	98.58	76.50	0.08	9222.60	4076.20	0.51	13007.99
		n	22	22	22	22	22	22	22
	RMH	Mean	328.36	227.06	0.69	10850.40	6147.43	1.77	16997.83
		SD	55.74	45.06	0.07	3962.61	2091.33	0.30	5914.17
		n	41	41	41	41	41	41	41
	SH	Mean	515.71	405.87	0.78	27040.94	16304.64	1.61	43345.59
		SD	90.00	85.24	0.04	10502.53	4499.77	0.31	14690.21
		n	7	7	7	7	7	7	7
50%	Other MP	Mean	555.80	458.40	0.83	35674.60	17429.60	2.09	53104.20
		SD	108.26	73.53	0.06	12973.26	6623.10	0.34	19210.72
		n	5	5	5	5	5	5	5
	Neanderthals	Mean	513.14	390.57	0.76	31213.36	13424.29	2.27	44616.14
		SD	88.39	74.94	0.06	13026.39	4282.12	0.42	16951.20
		n	14.00	14.00	14.00	14.00	14.00	14.00	14.00
	EMH	Mean	637.83	478.33	0.75	45803.17	21566.17	2.14	67369.67
		SD	58.38	29.36	0.05	8151.99	3563.85	0.30	10861.02
		n	6	6	6	6	6	6	6
	UP	Mean	470.46	369.54	0.78	32203.50	11531.36	2.73	41288.75
		SD	111.89	97.81	0.06	17428.04	5063.28	0.73	19981.39
		n	28	28	28	28	28	28	28
	RMH	Mean	374.98	258.61	0.69	15438.16	7442.22	2.39	22880.39
		SD	65.90	49.00	0.08	5943.88	2761.61	2.32	8488.46
		n	41	41	41	41	41	41	41
	SH	Mean	575.93	448.97	0.78	38814.11	17317.87	2.18	56131.94
		SD	95.89	71.11	0.04	14529.65	4274.11	0.45	18379.74
		n	7	7	7	7	7	7	7
65%	Neanderthals	Mean	660.63	433.63	0.65	50158.13	19177.50	2.57	69335.63
		SD	76.99	113.65	0.11	16532.29	4714.11	0.42	20956.83
		n	8	8	8	8	8	8	8
	EMH	Mean	700.80	472.40	0.68	60272.20	21377.60	2.85	81649.80
		SD	104.77	53.35	0.06	16779.84	5342.50	0.41	21454.96
		n	5	5	5	5	5	5	5
	UP	Mean	522.21	350.47	0.67	35918.11	11934.58	2.94	47852.68
		SD	119.33	86.23	0.07	16898.12	4811.41	0.41	21544.87
		n	19	19	19	19	19	19	19
	RMH	Mean	463.53	265.62	0.58	22118.47	9925.22	2.23	32043.69
		SD	90.52	49.07	0.07	8567.56	3645.64	0.36	11994.92
		n	41	41	41	41	41	41	41
	SH	Mean	694.26	464.32	0.67	57048.64	21110.62	2.69	78159.26
		SD	81.76	65.85	0.04	15056.35	4440.20	0.39	18806.54
		n	5	5	5	5	5	5	5
80%	Neanderthals	Mean	990.00	422.67	0.43	81647.00	34384.33	2.41	116031.33
		SD	93.79	8.08	0.04	10848.65	5796.64	0.47	13818.24
		n	3	3	3	3	3	3	3
	EMH	Mean	897.75	459.5	0.52	85,162	30509.25	2.8242237	115671.25
		SD	216.02	78.98	0.05	38649.39	11743.35	0.55	49408.59
		n	4	4	4	4	4	4	4
	UP	Mean	709.2	358.4	0.5	50751.9	19952.1	2.5	129779.9
		SD	144.79	90.28	0.13	24008.81	6780.65	0.50	219421.52
		n	13	13	13	13	13	13	13
	RMH	Mean	701.81	240.51	0.35	32781.53	15882.05	2.24	47774.51
		SD	154.07	47.03	0.06	13531.23	6874.50	0.87	19577.21
		n	40	40	40	40	40	40	40
	SH	Mean	963.60	416.48	0.43	86304.70	30627.03	2.80	116931.73
		SD	149.18	67.25	0.05	23525.86	7690.79	0.22	30960.81
		n	4	4	4	4	4	4	4

Abbreviations: EMH = Middle Pleistocene modern humans; UP = Early and Middle Upper Paleolithic; RMH = recent modern humans; SH = Sima de los Huesos; Other MP = Middle Pleistocene; TA = Total Area; CA = Cortical Area; Imax = Second moments of area—maximum; Imin = second moments of area—minimum; J = polar moment of area.

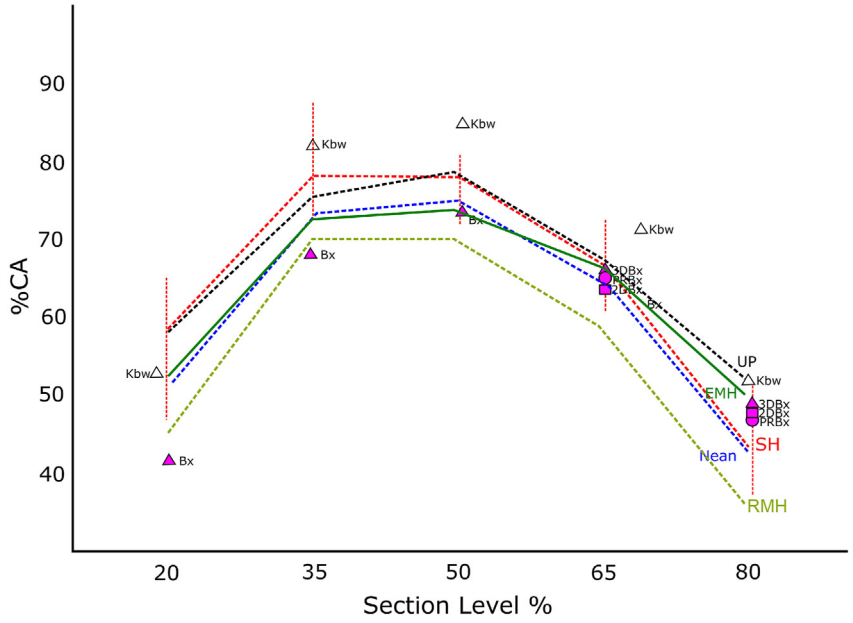

Figure 8. Tibia mean %CA variation for Neanderthals (Nean; blue dotted line), Sima de los Huesos (SH; red dotted line for the mean and vertical lines for the SH range), MP modern humans (EMH; dark green solid line), recent modern humans (RMH; light green dotted line), and Kabwe, Broken Hill (Kbw: NHMUK PA EM 691; open white triangles), in comparison to Boxgrove 1 (Bx; NHMUK PA EM 3566; solid pink triangles). (For interpretation of the references to color in this figure legend, the reader is referred to the Web version of this article.)

permanent mandibular incisors means that the potential of pulp shape for taxonomic and phylogenetic assessment is currently not possible statistically. We emphasize that if undertaken, wear should also be considered a factor impacting radicular pulp shape (Philippas, 1961).

Turning to the root dimensions, Boxgrove shows higher similarities to the SH material. They are more gracile than the incisors of Mauer, Neanderthals, and any Early and Middle Pleistocene hominin studied here, and more robust than the RMH samples. In addition, Boxgrove and SH share a relatively narrower labiolingual root diameter as well as a shorter incisor root, which places them in an intermediate position between the RMH sample and other extinct hominins, including other European hominins such as Mauer and later Neanderthals. Notably, our adjusted Z-Scores strongly align

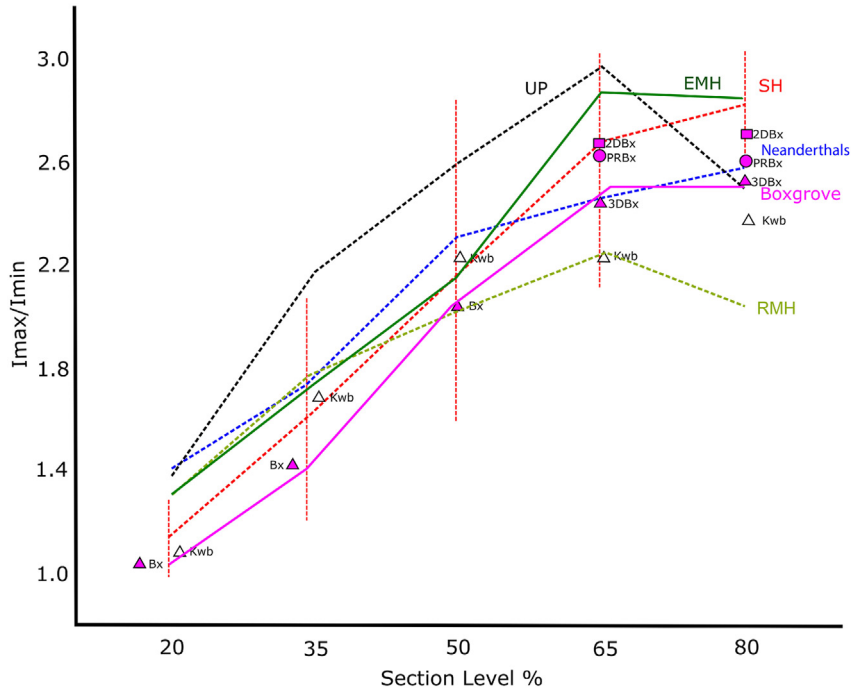

Figure 9. Tibia Imax/Imin variation in Neanderthals (blue dotted line), Sima de los Huesos (SH; dotted red line for the mean and vertical lines for the SH range), MP modern humans (EMH, dark green solid line), recent modern humans (RMH; light green dotted line), and Kabwe, Broken Hill (Kbw: NHMUK PA EM 691; open white triangles), in comparison to Boxgrove 1 (Bx: NHMUK PA EM 3566; solid pink triangles and line). (For interpretation of the references to color in this figure legend, the reader is referred to the Web version of this article.)

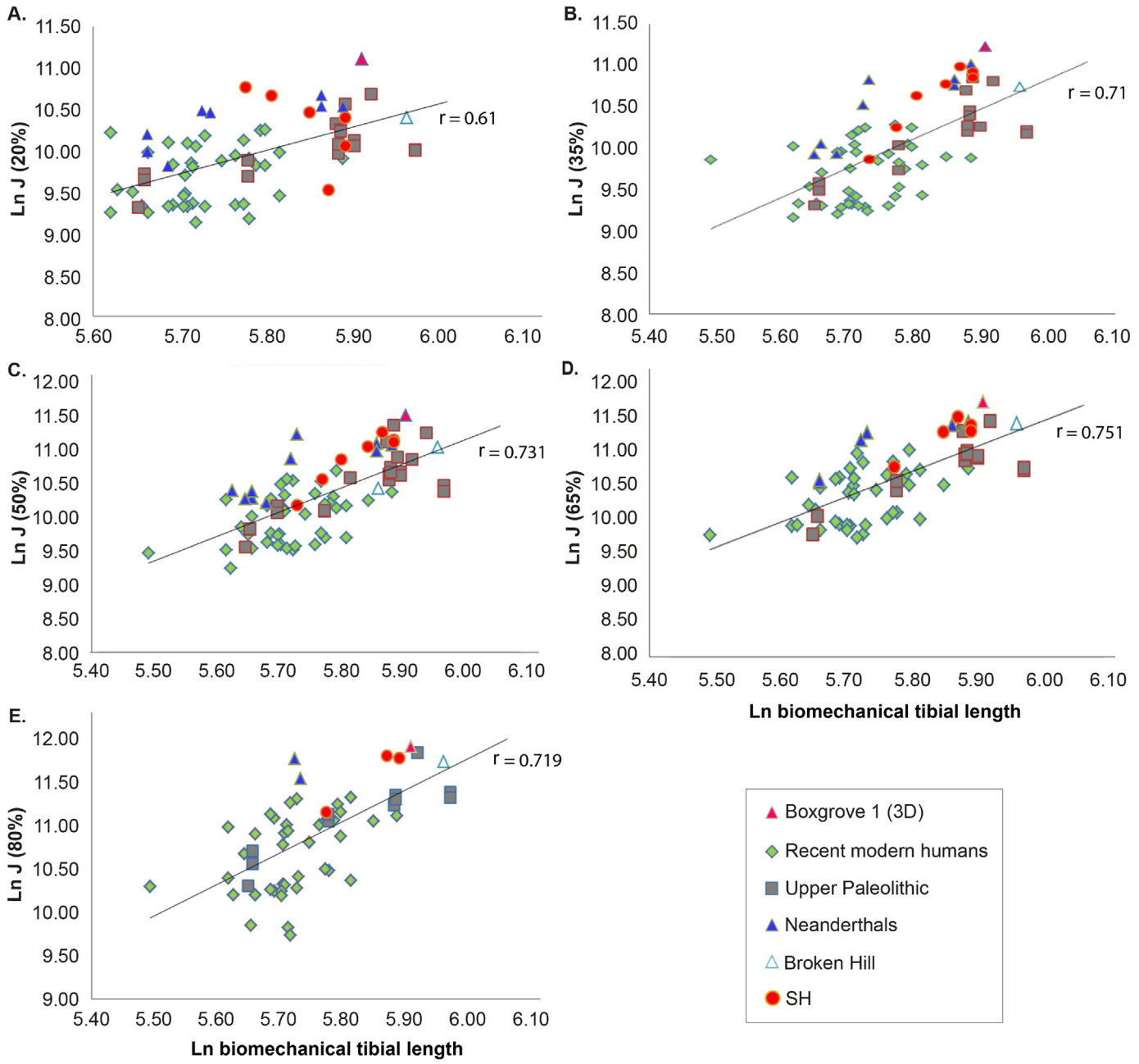

Figure 10. Tibia Ln J on Ln biomechanical tibial length. 20% section (A), 35% section (B), 50% section (C), 65% section (D), 80% section (E) Boxgrove 1 (NHMUK PA EM 3566: Boxgrove PR pink circle, Boxgrove 2D pink square, Boxgrove 3D pink triangle); Recent modern humans (RMH; light green diamonds); Early and Middle Upper Paleolithic (UP; gray squares); Neanderthals (blue triangles); Broken Hill (NHMUK PA EM 691; white triangle); Sima de los Huesos (SH; Tib-I, Tib-III, Tib-IV, Tib-VI, Tib-XI, Tib-XII, and AT-848; red dots). (For interpretation of the references to color in this figure legend, the reader is referred to the Web version of this article.)

Boxgrove and SH together for CA, RL, and RV relative to RMH and Neanderthals. Our study reveals that Boxgrove and SH are different from late Neanderthals, which share with other Early and Middle Pleistocene groups a more robust conformation. Our findings concur with those of Le Cabec et al. (2013) in that Neanderthals preserve the primitive condition, shared with other Early and Middle Pleistocene groups (*H. erectus*: S7_50, '*H. ergaster*': KNW-WT 1500, *H. antecessor*: Gran Dolina-TD6-2, *H. heidelbergensis*: Mauer). In this context, Boxgrove and SH would diverge from the primitive condition, supporting previous remarks on the high morphological variability in the MP and the possibility of more than one lineage coexisting during this period in Europe (Bermúdez de Castro et al., 2018; Martínez de Pinillos et al., 2020).

The analysis of the lower incisors does not justify the separation of SH and Boxgrove into distinct paleodemes. However, it must be noted that mandibles and dentitions within the same specimen may show different signals (Roksandic et al., 2011; Vialet et al., 2018). As an example, the Montmaurin mandible shows clear dental Neanderthal-like traits, whereas this pattern is less pronounced in the mandibular bone (Vialet et al., 2018). In contrast, in the SH fossils, presumably older than Mountmaurin-La Niche, both the teeth and the mandibles show clear Neanderthal affinities (Martinón-Torres et al., 2012; Arsuaga et al., 2014). Along the same line, the late MP specimen from Mala Balanica (Serbia) lacks Neanderthal apomorphies in both the mandible and the dentition (Roksandic et al., 2011) and the Arago specimens, roughly

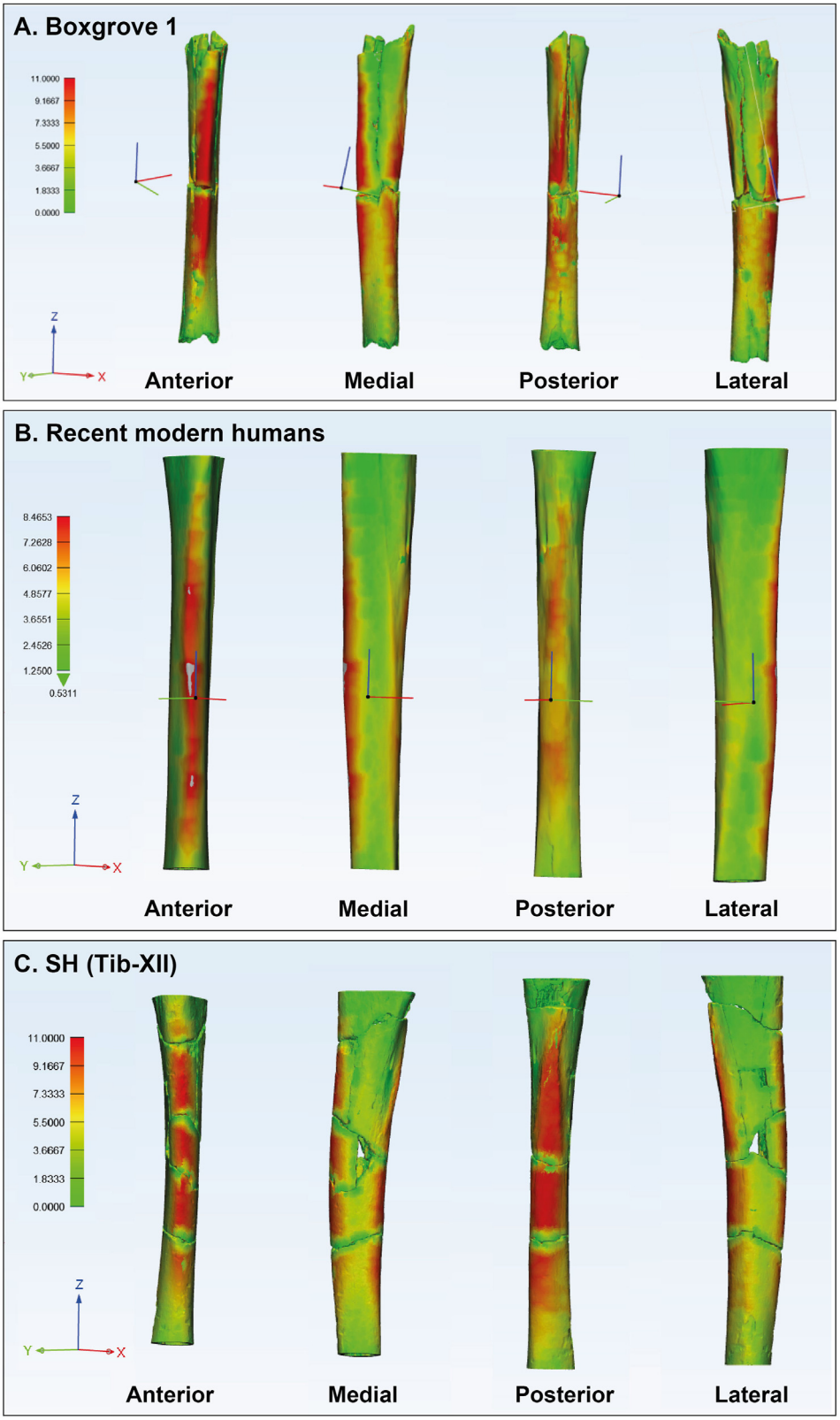

Figure 11. Wall thickness analysis in A) Boxgrove 1 (NHMUK PA EM 3566); B) recent modern humans; and (C) SH (Tib-XII). Color scale: from thickest (red) to thinnest (green) bone cortex.

contemporaneous with SH, show milder expressions of Neanderthal-like traits in both the mandible and the teeth (Bermúdez de Castro et al., 2018). This mosaic of features within the same specimens reinforces the notion of high morphological variability during the MP of Europe (Dennell et al., 2011). Overall, MP hominins from Europe show a general shared bauplan that suggests inclusion in the same clade, a clade from which the Neanderthal species would eventually emerge (Rosas and Bermúdez de Castro, 1998; Bermúdez de Castro et al., 2016, 2018). The closer similarities of the Boxgrove incisors to SH rather than to Gran Dolina-TD6 would support their grouping into the same evolutionary clade. It has been shown that the origin of some Neanderthal-like traits can be traced back to the European Early Pleistocene groups (Martinón-Torres et al., 2019), and a recent study of the dental remains from Fontana Ranuccio and Visogliano (Italy) showed that a Neanderthal-like inner dental structure, distinct from that of modern humans, was already present in MP populations at least 430 to 450 ka ago (Zanolli et al., 2018). However, with regard to the lower incisors, SH and Boxgrove show a more derived state, whereas Mauer and TD6 retain more primitive features. Nevertheless, establishing a species-level distinction among the MP specimens is difficult because of the scarcity and discontinuity of the fossil record. It is also important to recognize the limited utility of isolated teeth, particularly lower incisors, for taxonomic purposes.

4.2. Contrasts between Boxgrove 1 and Sima de los Huesos tibial morphology: Indicators of distinct Middle Pleistocene populations?

Boxgrove 1 is part of the diaphysis of a left tibia, without the distal and proximal epiphyses, deriving from an individual with an estimated stature of 177.3 ± 4.15 cm, which is taller than Neanderthals and SH individuals (Carretero et al., 2012). It differs from the RMH tibiae used for comparison in the present study, and is more similar to those of SH and Neanderthals in having thicker cortices and thicker bone walls in the anterior and posterior surfaces, a pattern shared with SH specimens. In relation to external morphology, it shows a strong and well-developed soleal line, indicating robust musculature attaching to that surface, plus a slight anteroposterior curvature. However, it is similar to modern humans in having a straight anterior tibial crest and the suggestion of a lateral concavity, which also fits with the plesiomorphic pattern, also present in Broken Hill, '*H. georgicus*,' and *H. floresiensis*. These features might therefore be a set of primitive traits for the genus *Homo*.

Cortical distribution in Boxgrove 1 (%CA) is similar to the Broken Hill tibia (Fig. 8). Diaphyseal shape pattern (Imax/Imin) is similar to those of SH, Neanderthals, and EMH (Fig. 9), but different from RMH and UP humans. Bone robusticity is higher than in any other individual studied in the comparative sample, which could be due to a larger body size and/or a higher activity pattern, as the Imax/Imin index suggests. This index is likely related to activity patterns in those hominins (Rodríguez et al., 2018), showing the active life of the Boxgrove 1 hominin.

Although the enhanced robusticity of the Boxgrove tibia could reflect a greater body mass and elevated activity levels, shape and surface feature contrasts between Boxgrove and SH suggest a level of population difference, whether recognized specifically or not. Thus, the Boxgrove tibial shaft shares with SH and Neanderthal traits that are absent in RMH, traits that are probably plesiomorphies linked to its robusticity. In addition, Boxgrove also lacks the SH and Neanderthal apomorphies in the curvature of the shaft and the morphology of the anterior tibial crest, which also points to its plesiomorphic status.

5. Conclusions

When the Boxgrove finds were made and described in the 1990s, there was much less material known and published from the MP of Europe, and the provisional assignment of the Boxgrove fossils to *H. heidelbergensis* was made more on chronological than morphological grounds. We are fortunately in a much better position now in terms of fossil material, but the intervening years have also led to a growing realization of the complexity of human evolution during the MP, with the apparent co-existence of different human lineages/species, and the taxonomically mosaic anatomies found in some of the fossils.

Compared with the clear similarities between Boxgrove and SH in the lower incisors, there is more basis for distinguishing the Boxgrove tibia at a population level in its particular combination of traits otherwise found in SH, Neanderthals, and modern humans. However, the primarily primitive morphology of the Boxgrove tibial shaft would fit that of the predicted last common ancestor for modern humans and Neanderthals (the last pre-split species). Based on the patterns observed here, there is no justification for assigning the Boxgrove and SH incisors to distinct paleodemes, but the tibial data show greater contrasts and suggest that these tibial specimens are unlikely to represent the same population. Thus, if the Boxgrove incisors and tibia represent a single population, their combination of traits suggests this paleodeme was distinct from the SH paleodeme.

Declaration of competing interest

All authors have no conflict of interest to disclose.

Acknowledgments

We acknowledge the members of the Atapuerca Research Team, with special thanks to those who excavate at Sima de los Huesos; the Conservation and Restoration Department at CENIEH, in particular to Pilar Fernández-Colón, for their assistance during the preparation and scanning of the material; Clément Zanolli, Federico Bernardini and Claudio Tuniz, from the Multidisciplinary Laboratory of the International Centre for Theoretical Physics in Trieste, for scanning part of the comparative collection; and Bernardo Perea, Elena Labajo and José Antonio Sánchez, from the Escuela de Medicina Legal, for granting access to the modern dental collection. We very much appreciate the help of Clément Zanolli in reconstructing the roots of the two Boxgrove incisors. M.-M.T. has received support from the Leakey Foundation through the personal support of Gordon Getty (2013) and Dub Crook (2014–2022). For the curation of *Homo neanderthalensis*, we thank Thüringisches Landesamt für Archäologische Denkmalpflege mit Museum für Ur- und Frühgeschichte and the Croatian Natural History Museum. This study has been supported by the Ministry of Ciencia e Innovación, [grant numbers: nº PGC2018-093925-B-C31-C33, Fondos Feder; and PDI2021-122355NB-C31-C33]. A.L.L. is the beneficiary of Deutsche Forschungsgemeinschaft and L.M.-F. has received support from the Spanish Ministry of Science and Innovation through the 'Maria de Maeztu' excellence accreditation (CEX2019-000945-M) and currently the Spanish Ministry of Science and Innovation through the 'Juan de la Cierva Incorporación' program. Part of this research was performed at the CENIEH-ICTS. The μCT scan of SH specimens was performed in the CENIEH Microscopy Laboratory by L.M.-F. and with the collaboration of the CENIEH staff. We also wish to acknowledge Jose Miguel Carretero and Rebeca Garcia (Universidad de Burgos) and Elena Santos (Universidad Complutense de Madrid), for their support with the CT scan. The Boxgrove project was funded by Historic England (English Heritage) with support

from the Institute of Archaeology, University College London, under the overall direction of Mark Roberts. The research of S.P. and C.S. is supported by the Calleva Foundation, and for C.S., the Human Origins Research Fund, and they wish to thank many present and former members of Natural History Museum London staff for their assistance, including Robert Kruszynski, Lorraine Cornish, Louise Humphrey, Rachel Ives, and Andy Currant.

Author contributions

A.L.L., L.R., M.M.-T., L.M.-F., J.M.B.C., and J.L.A conducted the analyses. S.P. and M.P. provided background, geoarchaeological context, and dating framework for the Boxgrove palaeolandscape and for the hominin locality Q1/B. All authors contributed to the writing of the manuscript.

Appendix A. Supplementary Online Material

Supplementary online material to this article can be found online at https://doi.org/10.1016/j.jhevol.2022.103253.

References

Abràmoff, M.D., Magalhães, P.J., Ram, S.J., 2004. Image processing with ImageJ. Biophotonics Int 11, 36–42.
Aguirre, E., de Lumley, M.-A., 1977. Fossil men from Atapuerca, Spain: Their bearing on human evolution in the Middle Pleistocene. J. Hum. Evol. 6, 681–688.
Aguirre, E., Basabe, J.M., Torres, T., 1975. Los fósiles humanos de Atapuerca (Burgos): Nota preliminar. Zephyrus: Revista de Prehistoria y Arqueología 26, 489–512.
Arnold, L.J., Demuro, M., Parés, J.M., Arsuaga, J.L., Aranburu, A., Bermúdez de Castro, J.M., Carbonell, E., 2014. Luminescence dating and palaeomagnetic age constraint on hominins from Sima de los Huesos, Atapuerca, Spain. J. Hum. Evol. 67, 85–107.
Arsuaga, J.L., Martínez, I., Gracia, A., Carretero, J.M., Lorenzo, C., García, N., Ortega, A.I., 1997. Sima de los Huesos (Sierra de Atapuerca, Spain). The site. J. Hum. Evol. 33, 109–127.
Arsuaga, J.L., Martínez, I., Arnold, L.J., Aranburu, A., Gracia-Téllez, A., Sharp, W.D., Quam, R.M., Falguères, C., Pantoja-Pérez, A., Bischoff, J., Poza-Rey, E., Parés, J.M., Carretero, J.M., Demuro, M., Lorenzo, C., Sala, N., Martinón-Torres, M., García, N., Alcázar De Velasco, A., Cuenca-Bescós, G., Gómez-Olivencia, A., Moreno, D., Pablos, A., Shen, C.C., Rodríguez, L., Ortega, A.I., García, R., Bonmatí, A., Bermúdez De Castro, J.M., Carbonell, E., 2014. Neandertal roots: cranial and chronological evidence from Sima de los Huesos. Science 344, 1358–1363.
Arsuaga, J.L., Carretero, J.M., Lorenzo, C., Gómez-Olivencia, A., Pablos, A., Rodríguez, L., García-González, R., Bonmatí, A., Qua, R.M., Pantoja-Pérez, A., Martínez, I., Aranburu, A., Gracia-Téllez, A., Poza-Rey, E., Sala, N., García, N., De Velasco, A.A., Cuenca-Bescós, G., Bermúdez De Castro, J.M., Carbonell, E., 2015. Postcranial morphology of the middle Pleistocene humans from Sima de los Huesos, Spain. Proc. Natl. Acad. Sci. USA 112, 11524–11529.
Bailey, S., 2006. Beyond shovel-shaped incisors: Neandertal dental morphology in a comparative context. Period. Biol. 108, 253–267.
Bayle, P., Alcaraz, M., Le Luyer, M., Robson Brown, K.A., 2017. The Palomas dental remains: enamel thickness and tissue proportions. In: Trinkaus, E., Walker, M.J. (Eds.), The People of Palomas: Neandertals from the Sima de Las Palomas Del Cabezo Gordo, Southeastern Spain. Texas A&M University Press, College Station, pp. 115–137.
Bermúdez de Castro, J.M., Martinón-Torres, M., Carbonell, E., Sarmiento, S., Rosas, A., Van Der Made, J., Lozano, M., 2004. The Atapuerca sites and their contribution to the knowledge of human evolution in Europe. Evol. Anthropol. 13, 25–41.
Bermúdez de Castro, J.M., Martinón-Torres, M., Rosell, J., Blasco, R., Arsuaga, J.L., Carbonell, E., 2016. Continuity versus discontinuity of the human settlement of Europe between the late Early Pleistocene and the early Middle Pleistocene. The mandibular evidence. Quat. Sci. Rev. 153, 51–62.
Bermúdez de Castro, J.M., Martinón-Torres, M., Martínez de Pinillos, M., García-Campos, C., Modesto-Mata, M., Martín-Francés, L., Arsuaga, J.L., 2018. Metric and morphological comparison between the Arago (France) and Atapuerca-Sima de los Huesos (Spain) dental samples, and the origin of Neanderthals. Quat. Sci. Rev. 217, 45–61.
Bermúdez de Castro, J.M., Martínez, I., Gracia-Téllez, A., Martinón-Torres, M., Arsuaga, J.L., 2021. The Sima de los Huesos Middle Pleistocene hominin site (Burgos, Spain). Estimation of the number of individuals. Anat. Rec. 304, 1463–1477.
Brabant, H., Sahly, A., 1964. Étude des dents néanderthaliennes découvertes dans la Grotte du Portel en Ariège (France). Bulletin du Groupement Internationale de la Recherche Scientifique en Stomatologie 7, 237–254.
Buti, L., Le Cabec, A., Panetta, D., Tripodi, M., Salvadori, P.A., Hublin, J.J., Feeney, R.N., Benazzi, S., 2017. 3D enamel thickness in Neandertal and modern human permanent canines. J. Hum. Evol. 113, 162–172.
Carbonell, E., Mosquera, M., 2006. The emergence of a symbolic behaviour: The sepulchral pit of Sima de los Huesos, Sierra de Atapuerca, Burgos, Spain. C. R. Palevol. 5, 155–160.
Carretero, J.M., Rodríguez, L., García-González, R., Arsuaga, J.L., Gómez-Olivencia, A., Lorenzo, C., Bonmatí, A., Gracia, A., Martínez, I., Quam, R., 2012. Stature estimation from complete long bones in the Middle Pleistocene humans from the Sima de los Huesos, Sierra de Atapuerca (Spain). J. Hum. Evol. 62, 242–255.
Cuenca-Bescós, G., Conesa, C.L., Canudo, J.I., Arsuaga, J.L., 1997. Small mammals from Sima de los Huesos. J. Hum. Evol. 33, 175–190.
Daura, J., Sanz, M., Arsuaga, J.L., Hoffmann, D.L., Quam, R.M., Ortega, M.C., Santos, E., Gómez, S., Rubio, A., Villaescusa, L., Souto, P., Mauricio, J., Rodrigues, F., Ferreira, A., Godinho, P., Trinkaus, E., Zilhão, J., 2017. New Middle Pleistocene hominin cranium from Gruta da Aroeira (Portugal). Proc. Natl. Acad. Sci. USA 114, 3397–3402.
Dean, D., Hublin, J.J., Holloway, R., Ziegler, R., 1998. On the phylogenetic position of the pre-Neandertal specimen from Reilingen, Germany. J. Hum. Evol. 34, 485–508.
Demuro, M., Arnold, L.J., Aranburu, A., Sala, N., Arsuaga, J.L., 2019. New bracketing luminescence ages constrain the Sima de los Huesos hominin fossils (Atapuerca, Spain) to MIS 12. J. Hum. Evol. 131, 76–95.
Dennell, R.W., Martinón-Torres, M., Bermúdez de Castro, J.M., 2011. Hominin variability, climatic instability and population demography in Middle Pleistocene Europe. Quat. Sci. Rev. 30, 1511–1524.
Falguères, C., Shao, Q., Han, F., Bahain, J.J., Richard, M., Perrenoud, C., Moigne, A.M., Lumley de, H., 2015. New ESR and U-series dating at Caune de l'Arago, France: A key-site for European Middle Pleistocene. Quat. Geochronol. 30, 547–553.
García, N., Arsuaga, J.L., Torres, T., 1997. The carnivore remains rrom the Sima de los Huesos Middle Pleistocene site (Sierra De Atapuerca, Spain). J. Hum. Evol. 33, 155–174.
García-Campos, C., Martinón-Torres, M., Martín-Francés, L., Modesto-Mata, M., Martínez de Pinillos, M., Arsuaga, J.L., Bermúdez de Castro, J.M., 2019. Enamel and dentine dimensions of the Pleistocene hominins from Atapuerca (Burgos, Spain): A comparative study of canine teeth. C.R. Palevol 18, 72–89.
Gardeisen, A., 1999. Middle Palaeolithic subsistence in the West Cave of "Le Portel" (Pyrénées, France). J. Archaeol. Sci. 26, 1145–1158.
Geraads, D., Hublin, J.J., Jaeger, J.J., Tong, H., Sen, S., Toubeau, P., 1986. The Pleistocene hominid site of Ternifine, Algeria: New results on the environment, age, and human industries. Quat. Res. 25, 380–386.
Gilbert, W.H., 2008. Daka member hominid postcranial remains. In: Gilbert, W.H., Asfaw, B. (Eds.), *Homo Erectus*: Pleistocene Evidence from the Middle Awash, Ethiopia. University of California Press, Berkeley, pp. 373–396.
Gómez-Olivencia, A., Carretero, J.M., Arsuaga, J.L., Rodríguez-García, L., García-González, R., Martínez, I., 2007. Metric and morphological study of the upper cervical spine from the Sima de los Huesos site (Sierra de Atapuerca, Burgos, Spain). J. Hum. Evol. 53, 6–25.
Gosman, J.H., Hubbell, Z.R., Shaw, C.N., Ryan, T.M., 2013. Development of cortical bone geometry in the human femoral and tibial diaphysis. Anat. Rec. 296, 774–787.
Kono, R.T., 2004. Molar enamel thickness and distribution patterns in extant great apes and humans: new insights based on a 3-dimensional whole crown perspective. Anthropol. Sci. 112, 121–146.
Harvati, K., Röding, C., Bosman, A.M., Karakostis, F.A., Grün, R., Stringer, C., Karkanas, P., Thompson, N.C., Koutoulidis, V., Moulopoulos, L.A., Gorgoulis, V.G., Kouloukoussa, M., 2019. Apidima Cave fossils provide earliest evidence of *Homo sapiens* in Eurasia. Nature 571, 500–504.
Hillson, S.W., Parfitt, S.A., Bello, S.M., Roberts, M.B., Stringer, C.B., 2010. Two hominin incisor teeth from the middle Pleistocene site of Boxgrove, Sussex, England. J. Hum. Evol. 59, 493–503.
Hublin, J.J., 2009. The origin of Neandertals. Proc. Natl. Acad. Sci. USA 106, 16022–16027.
Jungers, W.L., Larson, S.G., Harcourt-Smith, W., Morwood, M.J., Sutikna, T., Due Awe, R., Djubiantono, T., 2009. Descriptions of the lower limb skeleton of *Homo floresiensis*. J. Hum. Evol. 57, 538–554.
Kuhlwilm, M., Gronau, I., Hubisz, M.J., De Filippo, C., Prado-Martinez, J., Kircher, M., Fu, Q., Burbano, H.A., Lalueza-Fox, C., de La Rasilla, M., Rosas, A., Rudan, P., Krajkovic, D., Kucan, Z., Gušic, I., Marques-Bonet, T., Andrés, A.M., Viola, B., Pääbo, S., Meyer, M., Siepel, A., Castellano, S., 2016. Ancient gene flow from early modern humans into Eastern Neanderthals. Nature 530, 429–433.
Le Cabec, A., Gunz, P., Kupczik, K., Braga, J., Hublin, J.J., 2013. Anterior tooth root morphology and size in Neanderthals: Taxonomic and functional implications. J. Hum. Evol. 64, 169–193.
Lisiecki, L.E., Raymo, M.E., 2005. A Pliocene-Pleistocene stack of 57 globally distributed benthic δ 18O records. Paleoceanography 20, 1–17.
Lockey, A.L., Alemseged, Z., Hublin, J.-J., Skinner, M.M., 2020. Maxillary molar enamel thickness of Plio-Pleistocene hominins. J. Hum. Evol. 142, 102731.
Lockey, A.L., Martín-Francés, L., Arsuaga, J.L., Bermúdez de Castro, J.M., Martinón-Torres, M., 2022. Dental tissue proportions and linear dimensions of Sima de los Huesos lower incisors. Am. J. Biol. Anthropol. (Under review).
Lordkipanidze, D., Jashashvili, T., Vekua, A., De León, M.S.P., Zollikofer, C.P.E., Rightmire, G.P., Pontzer, H., Ferring, R., Oms, O., Tappen, M., Bukhsianidze, M., Agusti, J., Kahlke, R., Kiladze, G., Martinez-Navarro, B., Mouskhelishvili, A., Nioradze, M., Rook, L., 2007. Postcranial evidence from early *Homo* from Dmanisi, Georgia. Nature 449, 305–310.

Lorenzo, C., Carretero, J.M., Arsuaga, J.L., Gracia, A., Martínez, I., 1998. Intrapopulational body size variation and cranial capacity variation in Middle Pleistocene humans: The Sima de los Huesos sample (Sierra de Atapuerca, Spain). Am. J. Phys. Anthropol. 106, 19–33.
Macchiarelli, R., Bayle, P., Bondioli, L., Mazurier, A., Zanolli, C., 2013. From outer to inner structural morphology in dental anthropology: integration of the third dimension in the visualization and quantitative analysis of fossil remains. In: Scott, R.G., Irish, J.D. (Eds.), Anthropological Perspectives on Tooth Morphology: Genetics, Evolution, Variation. Cambrdige University Press, Cambridge, pp. 250–277.
Martín-Albaladejo, M., Martinón-Torres, M., García-González, R., Arsuaga, J.L., Bermúdez de Castro, J.M., 2017. Morphometric analysis of Atapuerca-Sima de los Huesos lower first molars. Quat. Int. 433 (Part A), 156–162.
Martin, L., 1985. Significance of enamel thickness in hominoid evolution. Nature 314, 260–263.
Martin, R., Saller, K., 1957. Lehrbuch der Anthropologie. Gustav Fischer, Stuttgart.
Martín-Francés, L., Martinón-Torres, M., de Pinillos, M.M., García-Campos, C., Modesto-Mata, M., Zanolli, C., Rodríguez, L., Bermúdez de Castro, J.M., 2018. Tooth crown tissue proportions and enamel thickness in Early Pleistocene *Homo antecessor* molars (Atapuerca, Spain). PLoS One 13, e0203334.
Martín-Francés, L., Martinón-Torres, M., de Pinillos, M.M., García-Campos, C., Zanolli, C., Bayle, P., Modesto-Mata, M., Arsuaga, J.L., Bermúdez de Castro, J.M., 2020. Crown tissue proportions and enamel thickness distribution in the Middle Pleistocene hominin molars from Sima de los Huesos (SH) population (Atapuerca, Spain). PLoS One 15, e0233281.
Martínez de Pinillos, M., Martín-Francés, L., Bermúdez de Castro, J.M., García-Campos, C., Modesto-Mata, M., Martinón-Torres, M., Vialet, A., 2020. Inner morphological and metric characterization of the molar remains from the Montmaurin-La Niche mandible: The Neanderthal signal. J. Hum. Evol. 145, 102739.
Martinón-Torres, M., Bermúdez De Castro, J.M., Gómez-Robles, A., Prado-Simón, L., Arsuaga, J.L., 2012. Morphological description and comparison of the dental remains from Atapuerca-Sima de los Huesos site (Spain). J. Hum. Evol. 62, 7–58.
Martinón-Torres, M., Bermúdez de Castro, J.M., Martínez de Pinillos, M., Modesto-Mata, M., Xing, S., Martín-Francés, L., García-Campos, C., Wu, X., Liu, W., 2019. New permanent teeth from gran Dolina-TD6 (Sierra de Atapuerca). The bearing of *Homo* antecessor on the evolutionary scenario of Early and Middle Pleistocene Europe. J. Hum. Evol. 127, 93–117.
Maureille, B., Rougier, H., Houët, F., Vandermeersch, B., 2001. Les dents inférieures du néandertalien Regourdou 1 (site de Regourdou, commune de Montignac, Dordogne): Analyses métriques et comparatives. PALEO 1, 183–200.
Meyer, M., Fu, Q., Aximu-Petri, A., Glocke, I., Nickel, B., Arsuaga, J.L., Martínez, I., Gracia, A., Bermúdez de Castro, J.M., Carbonell, E., Pääbo, S., 2014. A mitochondrial genome sequence of a hominin from Sima de los Huesos. Nature 505, 403–406.
Meyer, M., Arsuaga, J.L., De Filippo, C., Nagel, S., Aximu-Petri, A., Nickel, B., Martínez, I., Gracia, A., Bermúdez de Castro, J.M., Carbonell, E., Viola, B., Kelso, J., Prüfer, K., Pääbo, S., 2016. Nuclear DNA sequences from the Middle Pleistocene Sima de los Huesos hominins. Nature 531, 504–507.
Molnar, S., 1971. Human tooth wear, tooth function and cultural variability. Am. J. Phys. Anthropol. 34, 175–189.
Mounier, A., Caparros, M., 2015. Le statut phylogénétique d'*Homo heidelbergensis* – étude cladistique des homininés du Pléistocène moyen. Bull. Mem. Soc. Anthropol. Paris. 27, 110–134.
Mounier, A., Marchal, F., Condemi, S., 2009. Is *Homo heidelbergensis* a distinct species? New insight on the Mauer mandible. J. Hum. Evol. 56, 219–246.
Nagurka, M.L., Hayes, W.C., 1980. An interactive graphics package for calculating cross-sectional properties of complex shapes. J. Biomech. 13, 59–64.
Nomade, S., Muttoni, G., Guillou, H., Robin, E., Scardia, G., 2011. First 40Ar/39Ar age of the Ceprano man (central Italy). Quat. Geochronol. 6, 453–457.
Ohman, J.C., 1993. Computer software for estimating cross-sectional geometric properties of long bones with concentric and eccentric elliptical models. J. Hum. Evol. 25, 217–227.
Olejniczak, A.J., Smith, T.M., Feeney, R.N.M., Macchiarelli, R., Mazurier, A., Bondioli, L., Rosas, A., Fortea, J., de la Rasilla, M., Garcia-Tabernero, A., Radovčić, J., Skinner, M.M., Toussaint, M., Hublin, J.J., 2008. Dental tissue proportions and enamel thickness in Neandertal and modern human molars. J. Hum. Evol. 55, 12–23.
Pablos, A., Pantoja-Pérez, A., Martínez, I., Lorenzo, C., Arsuaga, J.L., 2017. Metric and morphological analysis of the foot in the Middle Pleistocene sample of Sima de los Huesos (Sierra de Atapuerca, Burgos, Spain). Quat. Int. 433 (Part A), 103–113.
Pan, L., Dumoncel, J., De Beer, F., Hoffman, J., Thackeray, J.F., Duployer, B., Tenailleau, C., Braga, J., 2016. Further morphological evidence on South African earliest *Homo* lower postcanine dentition: enamel thickness and enamel dentine junction. J. Hum. Evol. 96, 82–96.
Philippas, G.G., 1961. Influence of occlusal wear and age on formation of dentin and size of pulp chamber. J. Dent. Res. 40, 1186–1198.
Pope, M.I., 2002. The Significance of Biface-rich Assemblages: An Examination of Behavioural Controls on Lithic Assemblage Formation in the Lower Palaeolithic. Ph.D. Dissertation, University of Southampton.
Prado-Simón, L., Martinón-Torres, M., Baca, P., Gómez-Robles, A., Lapresa, M., Carbonell, E., Bermúdes de Castro, J.M., 2011. A morphological study of the tooth roots of the Sima del Elefante mandible (Atapuerca, Spain): A new classification of the teeth -biological and methodological considerations. Anthropol. Sci. 120, 61–72.
Prado-Simón, L., Martinón-Torres, M., Baca, P., Olejniczak, A.J., Gómez-Robles, A., Lapresa, M., Luis Arsuaga, J., Bermúdez de Castro, J.M., 2012. Three-dimensional evaluation of root canal morphology in lower second premolars of Early and Middle Pleistocene human populations from Atapuerca (Burgos, Spain). Am. J. Phys. Anthropol. 147, 452–461.
Preece, R.C., Parfitt, S.A., 2012. The Early and early Middle Pleistocene context of human occupation and lowland glaciation in Britain and northern Europe. Quat. Int. 271, 6–28.
Quam, R., Lorenzo, C., Martínez, I., Gracia-Téllez, A., Arsuaga, J.L., 2016. The bony labyrinth of the middle Pleistocene Sima de los Huesos hominins (Sierra de Atapuerca, Spain). J. Hum. Evol. 90, 1–15.
Rightmire, G.P., 2008. *Homo* in the Middle Pleistocene: Hypodigms, variation, and species recognition. Evol. Anthropol. 17, 8–21.
Rink, W.J., Mercier, N., Mihailović, D., Morley, M.W., Thompson, J.W., Roksandic, M., 2013. New Radiometric ages for the BH-1 hominin from Balanica (Serbia): Implications for understanding the oole of the Balkans in Middle Pleistocene human evolution. PLoS One 8, e54608.
Roberts, M.B., Parfitt, S.A., 1999. Boxgrove: A middle Pleistocene Hominid Site at Eartham Quarry, Boxgrove, West Sussex. English Heritage Archaeological Report 17, London.
Roberts, M., Pope, M., 2009. The archaeological and sedimentary records from Boxgrove and Slindon. Mollusca 172, 71–80.
Roberts, M.B., Stringer, C.B., Parfitt, S.A., 1994. A hominid tibia from Middle Pleistocene sediments at Boxgrove, UK. Nature 369, 311–313.
Rodríguez, L., Carretero, J.M., García-González, R., Lorenzo, C., Gómez-Olivencia, A., Quam, R., Martínez, I., Gracia-Téllez, A., Arsuaga, J.L., 2016. Fossil hominin radii from the Sima de los Huesos Middle Pleistocene site (Sierra de Atapuerca, Spain). J. Hum. Evol. 90, 55–73.
Rodríguez, L., Carretero, J.M., García-González, R., Arsuaga, J.L., 2018. Cross-sectional properties of the lower limb long bones in the Middle Pleistocene Sima de los Huesos sample (Sierra de Atapuerca, Spain). J. Hum. Evol. 117, 1–12.
Roksandic, M., Mihailović, D., Mercier, N., Dimitrijević, V., Morley, M.W., Rakočević, Z., Mihailović, B., Guibert, P., Babb, J., 2011. A human mandible (BH-1) from the Pleistocene deposits of Mala Balanica cave (Sićevo Gorge, Niš, Serbia). J. Hum. Evol. 61, 186–196.
Roksandic, M., Radović, P., Lindal, J., 2018. Revising the hypodigm of *Homo heidelbergensis*: A view from the Eastern Mediterranean. Quat. Int. 466, 66–81.
Rosas, A., Bermúdez de Castro, J.M., 1998. The Mauer mandible and the evolutionary significance of *Homo heidelbergensis*. Geobios 31, 687–697.
Ruff, C.B., 1995. Biomechanics of the hip and birth in early *Homo*. Am. J. Phys. Anthropol. 98, 527–574.
Ruff, C.B., Hayes, W.C., 1983. Cross-sectional geometry of Pecos Pueblo femora and tibiae—a biomechanical investigation: I. Method and general patterns of variation. Am. J. Phys. Anthropol. 60, 359–381.
Ruff, C.B., Leo, F.P., 1986. Use of computed tomography in skeletal structure research. Am. J. Phys. Anthropol. 29, 181–196.
Ruff, C.B., Trinkaus, E., Walker, A., Larsen, C.S., 1993. Postcranial robusticity in *Homo*. I: temporal trends and mechanical interpretation. Am. J. Phys. Anthropol. 91, 21–53.
Ruff, C.B., Walker, A., Trinkaus, E., 1994. Postcranial robusticity in *Homo*. III: Ontogeny. Am. J. Phys. Anthropol. 93, 35–54.
Schoetensack, O., 1908. Der Unterkiefer des Homo heidelbergensis. Links 5, 5.
Scolan, H., Santos, F., Tillier, A.M., Maureille, B., Quintard, A., 2012. Des nouveaux vestiges néanderthaliens à Las Pélénos (Monsempron-Libos, Lot-et-Garonne, France). Bull. Mem. Soc. Anthropol. Paris. 24, 69–95.
Sjøvold, T., 1990. Estimation of stature from long bones utilizing the line of organic correlation. Hum. Evol. 5, 431–447.
Skinner, M.M., Alemseged, Z., Gaunitz, C., Hublin, J.-J., 2015. Enamel thickness trends in Plio-Pleistocene hominin mandibular molars. J. Hum. Evol. 85, 35–45.
Smith, T.M., Martin, L.B., Leakey, M.G., 2003. Enamel thickness, microstructure and development in *Afropithecus turkanensis*. J. Hum. Evol. 44, 283–306.
Smith, T.M., Olejniczak, A.J., Zermeno, J.P., Tafforeau, P., Skinner, M.M., Hoffmann, A., Radovčić, J., Toussaint, M., Kruszynski, R., Menter, C., Moggi-Cecchi, J., Glasmacher, U.A., Kullmer, O., Schrenk, F., Stringer, C., Hublin, J.J., 2012. Variation in enamel thickness within the genus *Homo*. J. Hum. Evol. 62, 395–411.
Streeter, M., Stout, S.D., Trinkaus, E., Stringer, C.B., Roberts, M.B., Parfitt, S.A., 2001. Histomorphometric age assessment of the Boxgrove 1 tibial diaphysis. J. Hum. Evol. 40, 331–338.
Stringer, C.B., 1983. Some further notes on the morphology and dating of the Petralona hominid. J. Hum. Evol. 12, 731–742.
Stringer, Chris, 2011. The Origin of Our Species. Allen Lane, London.
Stringer, C., 2012. The status of *Homo heidelbergensis* (Schoetensack 1908). Evol. Anthropol. 21, 101–107.
Stringer, C.B., Trinkaus, E., Roberts, M.B., Parfitt, S.A., Macphail, R.I., 1998. The Middle Pleistocene human tibia from Boxgrove. J. Hum. Evol. 34, 509–547.
Trinkaus, E., 2009. The human tibia from Broken Hill, Kabwe, Zambia. PaleoAnthropology 145, 165.
Trinkaus, E., Ruff, C., 2012. Femoral and tibial diaphyseal cross-sectional geometry in Pleistocene *Homo*. PaleoAnthropology 2012, 13–62.
Trinkaus, E., Stringer, C.B., Ruff, C.B., Hennessy, R.J., Roberts, M.B., Parfitt, S.A., 1999. Diaphyseal cross-sectional geometry of the Boxgrove 1 Middle Pleistocene human tibia. J. Hum. Evol. 37, 1–25.
Vialet, A., Modesto-Mata, M., Martinón-Torres, M., De Pinillos, M.M., Bermúdez de Castro, J.M., 2018. A reassessment of the Montmaurin-La Niche mandible

(Haute Garonne, France) in the context of European Pleistocene human evolution. PLoS One 13, e0189714.
Wagner, G.A., Krbetschek, M., Degering, D., Bahain, J.J., Shao, Q., Falguères, C., Voinchet, P., Dolo, J.M., Garcia, T., Rightmire, G.P., 2010. Radiometric dating of the type-site for *Homo heidelbergensis* at Mauer, Germany. Proc. Natl. Acad. Sci. USA 107, 19726–19730.
Walker, M.J., Gibert, J., López, M.V., Lombardi, A.V., Pérez-Pérez, A., Zapata, J., Ortega, J., Higham, T., Pike, A., Schwenninger, J.L., Zilhão, J., Trinkaus, E., 2008. Late Neandertals in Southeastern Iberia: Sima de las Palomas del Cabezo Gordo, Murcia, Spain. Proc. Natl. Acad. Sci. USA 105, 20631–20636.
Weniger, W.C., Döllner, J., Macchirelli, R., Mandel, M., Mayer, P., Radovic, J., Semal, P., 2005. TNT: the Neanderthal tools and NESPOS. In: Figueiredo, A., Velho, G. (Eds.), The World Is in Your Eyes: CAA2005: Computer Applications and Quantitative Methods in Archaeology: Proceedings of the 33rd Conference, Tomar, March 2005, pp. 267–269.
Whittaker, J., Parfitt, S., 2017. The palaeoenvironment of the important Middle Pleistocene hominin site at Boxgrove (West Sussex, UK) as delineated by the foraminifera and ostracods. In: Williams, M., Hill, T., Boomer, I., Wilkinson, I.P. (Eds.), The Archaeological and Forensic Applications of Microfossils: A Deeper Understanding of Human History. The Micropalaeontological Society, Special Publications. Geological Society, London, pp. 9–34.
Zanolli, C., Bayle, P., Macchiarelli, R., 2010. Tissue proportions and enamel thickness distribution in the early Middle Pleistocene human deciduous molars from Tighenif, Algeria. C. R. Palevol. 9, 341–348.
Zanolli, C., Mazurier, A., 2013. Endostructural characterization of the *H. heidelbergensis* dental remains from the early middle Pleistocene site of Tighenif, Algeria. C. R. Palevol. 12, 293–304.
Zanolli, C., Martinón-Torres, M., Bernardini, F., Boschian, G., Coppa, A., Dreossi, D., Mancini, L., De Pinillos, M.M., Martín-Francés, L., Bermúdez De Castro, J.M., Tozzi, C., Tuniz, C., Macchiarelli, R., 2018. The middle Pleistocene (MIS 12) human dental remains from Fontana Ranuccio (Latium) and Visogliano (Friuli-Venezia Giulia), Italy. A comparative high resolution endostructural assessment. PLoS One 13, e0189773.